

A Predictive and Testable Unified Theory of Fermion Masses, Mixing and Leptogenesis

Bowen Fu,^a Stephen F. King,^a Luca Marsili,^b Silvia Pascoli,^{b,c,d} Jessica Turner^e and Ye-Ling Zhou^{f,g}

^a*School of Physics and Astronomy, University of Southampton, Southampton, SO17 1BJ, U.K.*

^b*Dipartimento di Fisica e Astronomia, Università di Bologna, via Irnerio 46, 40126 Bologna, Italy*

^c*INFN, Sezione di Bologna, viale Berti Pichat 6/2, 40127 Bologna, Italy*

^d*CERN, Theoretical Physics Department, Geneva, Switzerland*

^e*Institute for Particle Physics Phenomenology, Department of Physics, Durham University, Durham DH1 3LE, U.K.*

^f*School of Fundamental Physics and Mathematical Sciences, Hangzhou Institute for Advanced Study, UCAS, Hangzhou, China*

^g*International Centre for Theoretical Physics Asia-Pacific, Beijing/Hangzhou, China*

E-mail: b.fu@soton.ac.uk, s.f.king@soton.ac.uk,
luca.marsili@studio.unibo.it, silvia.pascoli@unibo.it,
jessica.turner@durham.ac.uk, zhouyeling@ucas.ac.cn

ABSTRACT: We consider a minimal non-supersymmetric $SO(10)$ Grand Unified Theory (GUT) model that can reproduce the observed fermionic masses and mixing parameters of the Standard Model. We calculate the scales of spontaneous symmetry breaking from the GUT to the Standard Model gauge group using two-loop renormalisation group equations. This procedure determines the proton decay rate and the scale of $U(1)_{B-L}$ breaking, which generates cosmic strings and the right-handed neutrino mass scales. Consequently, the regions of parameter space where thermal leptogenesis is viable are identified and correlated with the fermion masses and mixing, the neutrinoless double beta decay rate, the proton decay rate, and the gravitational wave signal resulting from the network of cosmic strings. We demonstrate that this framework, which can explain the Standard Model fermion masses and mixing and the observed baryon asymmetry, will be highly constrained by the next generation of gravitational wave detectors and neutrino oscillation experiments which will also constrain the proton lifetime.

KEYWORDS: Grand Unification, Proton Decay, Cosmic Strings, Gravitational Waves

Contents

1	Introduction	1
2	The framework	3
2.1	Symmetry breaking of $SO(10)$	3
2.2	Matter Field Decomposition and Fermion Masses	4
2.3	Gauge Unification	8
3	Fermion masses and mixing	12
3.1	Parametrisation using Hermitian Yukawa matrices	13
3.2	Procedure of numerical analysis	15
3.3	The benchmark study	21
4	Leptogenesis	22
5	Testability of $SO(10)$ GUT and leptogenesis using gravitational waves	25
6	Discussion and conclusion	31

1 Introduction

Grand Unified Theories (GUTs) have long been an attractive framework for unifying the non-gravitational interactions. The minimal option, which can predict neutrino masses and mixing, uses the gauge group $SO(10)$. Several well-studied symmetries can be embedded in $SO(10)$, including $SU(5)$ [1], flipped $SU(5) \times U(1)$ [2–5] and the Pati-Salam model $SU(4)_c \times SU(2)_L \times SU(2)_R$ [6]. Thanks to this rich structure, there are many possible symmetry-breaking chains from $SO(10)$ down to the Standard Model (SM) gauge group, G_{SM} , most of them via the Pati-Salam symmetry [7]. An appealing feature of an intermediate Pati-Salam symmetry in non-supersymmetric GUTs is that gauge unification can be achieved, and there is an intermediate $U(1)_{B-L}$ subgroup which is spontaneously broken, generating right-handed neutrino masses. In addition to inducing light neutrino masses via the seesaw mechanism, the CP-violating and out-of-equilibrium decays of the right-handed neutrinos can produce the observed matter-antimatter asymmetry via thermal leptogenesis [8]. Moreover, the $U(1)_{B-L}$ symmetry breaking can also generate cosmic strings in the early Universe, which can intercommute and emit gravitational radiation forming a stochastic gravitational wave (GW) background that future GW interferometers can test.

The connection between GUTs and gravitational waves has been studied in [9] where the simple breaking pattern $SO(10) \rightarrow G_{SM} \times U(1)_{B-L} \rightarrow G_{SM}$ was shown to be consistent with inflation, leptogenesis, and dark matter, while the $U(1)_{B-L}$ symmetry breaking generates cosmic strings. The connection between high-scale thermal leptogenesis and GWs

was also pointed in [10] where it was assumed that the $U(1)_{B-L}$ breaking scale is the same as the seesaw and leptogenesis scales. In Ref. [11], we highlighted the complementarity between proton decay and gravitational wave signals from cosmic strings as a powerful method of probing GUTs. Subsequently, in Ref. [12], we studied all possible non-supersymmetric $SO(10)$ symmetry-breaking chains. We performed a comprehensive renormalisation group (RG) analysis to find the correlations between the proton decay rate and the GW signal. We also identified which chains survived the current non-observation of both proton decay and GWs and could be tested by future neutrino and GW experiments.

In this paper, we go beyond these works by providing a detailed study on a specific $SO(10)$ breaking chain that provides unification and predicts a proton decay width via the channel $p \rightarrow \pi^0 e^+$, consistent with the experimental bound of the Super-Kamiokande (Super-K) [13] and can be fully tested by future proton decay searches of Hyper-K [12]. Further, this breaking chain generates cosmic strings at the lowest intermediate scale, $M_1 \sim 10^{13}$ GeV. A GW background generated by such a string network is just around the corner and may be even already hinted at by recent observations in PTA experiments, including NANOGrav [14], PPTA [15], EPTA [16] and IPTA [17]. We determine the minimal necessary particle content to induce the pattern of breaking and perform an RG analysis and numerical fit of our model to SM data to postdict the fermion masses and mixing, including the mass scales of the right-handed neutrinos. As this procedure determines the scales of symmetry breaking of our model and the masses of the right-handed neutrinos, the matter-antimatter asymmetry associated with thermal leptogenesis is predicted. We then show that successful leptogenesis can occur in the regions of the model parameter space consistent with SM fermion masses and mixing and can be correlated with a GW signal and proton decay. Compared with [10], such an approach allows us to go beyond generic considerations and instead to quantitatively account for the hierarchy between the leptogenesis and see-saw scales, as well as with the $U(1)_{B-L}$ breaking scale, thanks to the constraints imposed by reproducing the low energy data. The latter scale is of particular interest since pulsar timing arrays such as PPTA [18] and NANOGrav [19] are sensitive to the predicted GW signals while future large-scale neutrino experiment, Hyper-Kamiokande (Hyper-K) [20], will be able to probe the predicted proton decay rate of this model. The correlation between these two observables will be a crucial test of our GUT model, and such methodology can be applied to other GUT models, presenting a new avenue to try to unveil the physics at very high scales.

This paper is organised as follows: in Section 2, we discuss the GUT symmetry breaking pattern and the particle content of our model, including fermionic and Higgs representations of the GUT and our RG running procedure. In Section 3, we discuss how we relate our model to the quark lepton data, our fitting procedure and the ensuing results. In Section 4, we discuss the basics of non-resonant thermal leptogenesis and how we determine the baryon asymmetry produced from the successful points in the model parameter space and in Section 5, we demonstrate that the regions of the model parameter space that yield successful leptogenesis and fermionic masses and mixing will be associated with a GW signal.

Finally, we summarise and discuss in Section 6. As a case study, we consider a benchmark point (referred to as BP1 throughout) and discuss how it satisfies all these experimental constraints in each section.

2 The framework

We focus on a breaking chain (classified as chain III4 of type (c) in Ref. [12]) that is of particular interest as it is currently allowed and predicts a proton decay rate testable by Hyper-K. We discuss the breaking chain's matter content and gauge unification in this section.

2.1 Symmetry breaking of $SO(10)$

We study the following breaking chain with three intermediate symmetries (G_3 , G_2 , and G_1):

$$\begin{aligned}
& SO(10) \\
& \mathbf{54} \downarrow \text{broken at } M_X \\
& G_3 \equiv SU(4) \times SU(2)_L \times SU(2)_R \times Z_2^C \\
& \mathbf{210} \downarrow \text{broken at } M_3 \\
& G_2 \equiv SU(3)_c \times SU(2)_L \times SU(2)_R \times U(1)_X \times Z_2^C \\
& \mathbf{45} \downarrow \text{broken at } M_2 \\
& G_1 \equiv SU(3)_c \times SU(2)_L \times SU(2)_R \times U(1)_X \\
& \mathbf{\bar{126}} \downarrow \text{broken at } M_1 \\
& G_{\text{SM}} \equiv SU(3)_c \times SU(2)_L \times U(1)_Y .
\end{aligned} \tag{2.1}$$

The boldface number beside the arrow indicates the Higgs representation of $SO(10)$, triggering the symmetry breaking. In this work, we follow the same convention as Ref. [12] where the GUT symmetry breaking scale is denoted as M_X and the mass scale of the subsequent breaking of the group G_I (for $I = 1, 2, 3$) is denoted as M_I .¹ All particles, except the gauge fields of the model, are listed in Table 1. We note that Z_2^C refers to the parity symmetry between left and right conjugation ($L \leftrightarrow R^c$, where c indicates charge conjugation) and that $U(1)_X$ is identical to the $U(1)_{B-L}$ symmetry with the charge correlated via $X = \sqrt{\frac{3}{2}}(\frac{B-L}{2})$. The correlations between $U(1)$ charges are given by $Y = \sqrt{\frac{3}{5}}(I_{3R} + \frac{B-L}{2})$, where I_{3R} is the isospin in $SU(2)_R$.

To achieve each step of symmetry breaking, i.e., $SO(10) \rightarrow G_3 \rightarrow G_2 \rightarrow G_1$, we include three Higgs multiplets, $\mathbf{54}$, $\mathbf{210}$, and $\mathbf{45}$ of $SO(10)$, respectively. These Higgs fields spontaneously break the GUT symmetry as follows:

¹However, we change the notation of the running energy scale to from μ to Q as the string tension is often denoted as μ .

	Multiplet	Role in the model
Fermions	16	Contains all SM fermions and RH neutrinos
Higgses	10	Generates fermion masses
	45	Triggers intermediate symmetry breaking
	54	Triggers GUT symmetry breaking
	120	Generates fermion masses
	$\overline{\mathbf{126}}$	Generates fermion masses & intermediate symmetry breaking
	210	Triggers intermediate symmetry breaking

Table 1: The $SO(10)$ representations of the fermion and Higgs particles of our $SO(10)$ GUT model and their roles.

- **54** contains a parity-even singlet $(\mathbf{1}, \mathbf{1}, \mathbf{1})$ of $G_3 \equiv SU(4)_c \times SU(2)_L \times SU(2)_R$ where each entry in the bracket $(\mathbf{r}_1, \mathbf{r}_2, \dots)$ refers to the field representation transforming in the group $G \equiv H_1 \times H_2 \times \dots$. Once $(\mathbf{1}, \mathbf{1}, \mathbf{1})$ gains a non-trivial vacuum expectation value (VEV) at scale M_X , $SO(10)$ is spontaneously broken to G_3 .
- In G_3 , **210** can be decomposed to $(\mathbf{15}, \mathbf{1}, \mathbf{1})_1$ of G_3 , which is further decomposed into a parity-even and trivial singlet $(\mathbf{1}, \mathbf{1}, \mathbf{1}, 0)_1$ of $SU(3)_c \times SU(2)_L \times SU(2)_R \times U(1)_X$, where the last entry in the bracket is the field charge in the $U(1)$ symmetry and the subscript is used to distinguish from another field with the same representation discussed below. The VEV of this singlet breaks G_3 to G_2 at scale M_3 .
- The breaking of G_2 to G_1 is realised via a **45** of $SO(10)$, which decomposed into $(\mathbf{15}, \mathbf{1}, \mathbf{1})_2$ of G_3 and a further $(\mathbf{1}, \mathbf{1}, \mathbf{1}, 0)_2$ of G_2 and G_1 . This singlet is parity-odd, and its VEV induces the breaking of $G_2 \rightarrow G_1$ at scale M_2 .
- Finally, the breaking of $G_1 \rightarrow G_{\text{SM}}$ at scale M_1 is provided by $\overline{\mathbf{126}}$, which is decomposed into a triplet $(\mathbf{1}, \mathbf{1}, \mathbf{3}, -1)$ of $SU(3)_c \times SU(2)_L \times SU(2)_R \times U(1)_X$ and to a further singlet, $(\mathbf{1}, \mathbf{1}, 0)$, of G_{SM} . This singlet field, denoted as ϕ_S , provides mass to the three right-handed neutrinos.

We summarise the decomposition of Higgses, which triggers the breaking of $SO(10)$ and intermediate symmetries, in Table 2.

2.2 Matter Field Decomposition and Fermion Masses

In order to assess if our model can predict the measured fermionic masses and mixing, it is important to understand the matter content of the breaking chain. Fermions are arranged as a **16** of $SO(10)$ and follow the decomposition given in Table 3 where L (R) denote the left-handed (right-handed) fermions of G_3 which contains the SM left-handed (right-handed) fermions where $Q_{L(R)}$ and $\ell_{L(R)}$ are the quark and leptonic $SU(2)_{L(R)}$ doublets, respectively, and u_R, d_R, e_R , and ν_R are the quark and lepton $SU(2)_L$ singlets, respectively.

$SO(10)$	54	210	45	$\overline{\mathbf{126}}$
G_3	$(\mathbf{1}, \mathbf{1}, \mathbf{1})$	$(\mathbf{15}, \mathbf{1}, \mathbf{1})_1$	$(\mathbf{15}, \mathbf{1}, \mathbf{1})_2$	$(\mathbf{10}, \mathbf{1}, \mathbf{3}) + (\overline{\mathbf{10}}, \mathbf{3}, \mathbf{1})$
G_2	–	$(\mathbf{1}, \mathbf{1}, \mathbf{1}, 0)_1$	$(\mathbf{1}, \mathbf{1}, \mathbf{1}, 0)_2$	$(\mathbf{1}, \mathbf{1}, \mathbf{3}, -1) + (\mathbf{1}, \mathbf{3}, \mathbf{1}, 1)$
G_1	–	–	$(\mathbf{1}, \mathbf{1}, \mathbf{1}, 0)_2$	$(\mathbf{1}, \mathbf{1}, \mathbf{3}, -1)$
G_{SM}	–	–	–	$(\mathbf{1}, \mathbf{1}, 0)_S$

Table 2: Decomposition of the Higgses which induce spontaneous symmetry breaking at each step of the breaking chain. Each Higgs (from left to right) is eventually decomposed to a singlet whose non-vanishing VEV preserves the symmetry G_I (for $I = 3, 2, 1, \text{SM}$) in the same row but breaks larger symmetries. The subscript distinguishes different fields of the same representation.

$SO(10)$	16
G_3	$(\mathbf{4}, \mathbf{2}, \mathbf{1})_L + (\overline{\mathbf{4}}, \mathbf{1}, \mathbf{2})_{R^c}$
G_2	$(\mathbf{3}, \mathbf{2}, \mathbf{1}, 1/6)_{Q_L} + (\overline{\mathbf{3}}, \mathbf{1}, \mathbf{2}, -1/6)_{Q_R^c}$ $+ (\mathbf{1}, \mathbf{2}, \mathbf{1}, -1/2)_{l_L} + (\mathbf{1}, \mathbf{1}, \mathbf{2}, 1/2)_{l_R^c}$
G_1	$(\mathbf{3}, \mathbf{2}, \mathbf{1}, 1/6)_{Q_L} + (\overline{\mathbf{3}}, \mathbf{1}, \mathbf{2}, -1/6)_{Q_R^c}$ $+ (\mathbf{1}, \mathbf{2}, \mathbf{1}, -1/2)_{l_L} + (\mathbf{1}, \mathbf{1}, \mathbf{2}, 1/2)_{l_R^c}$
G_{SM}	$(\mathbf{3}, \mathbf{2}, 1/6)_{Q_L} + (\overline{\mathbf{3}}, \mathbf{1}, -2/3)_{u_R^c} + (\overline{\mathbf{3}}, \mathbf{1}, 1/3)_{d_R^c}$ $+ (\mathbf{1}, \mathbf{2}, -1/2)_{l_L} + (\mathbf{1}, \mathbf{1}, 0)_{\nu_R^c} + (\mathbf{1}, \mathbf{1}, 1)_{e_R^c}$

Table 3: Decomposition of the matter multiplet **16** in each step of the breaking chain.

Three Higgs multiplets, **10**, $\overline{\mathbf{126}}$ and **120**, are required to generate the Standard Model fermion masses. Compared to Ref. [12], where we considered a minimal survival hypothesis [21], we include one additional Higgs (**120**) which is required to generate all fermion mass spectra, mixing angles, and CP-violating phases in the quark and lepton sectors. Here, $\overline{\mathbf{126}}$ is the same Higgs used in the breaking $G_1 \rightarrow G_{\text{SM}}$. For this breaking chain, we list decompositions of Higgs, which are responsible for mass generation in Table 2.

Applying this decomposition, we have two $(\mathbf{1}, \mathbf{2}, \mathbf{2})$ and two $(\mathbf{15}, \mathbf{2}, \mathbf{2})$ multiplets of G_3 after the $SO(10)$ breaking. These multiplets are composed of four bi-doublets, $(\mathbf{1}, \mathbf{2}, \mathbf{2}, 0)$, of G_2 and G_1 . After $SU(2)_R$ is broken below M_1 , each bi-doublet contains two electroweak doublets $(\mathbf{1}, \mathbf{2}, \mp 1/2)$, and eventually, we arrive at the eight electroweak doublets of the model which we denote as $h_i = \{\tilde{h}_{\mathbf{10}}^u, \tilde{h}_{\overline{\mathbf{126}}}^u, \tilde{h}_{\mathbf{120}}^u, \tilde{h}'_{\mathbf{120}}^u, h_{\mathbf{10}}^d, h_{\overline{\mathbf{126}}}^d, h_{\mathbf{120}}^d, h'_{\mathbf{120}}^d\}$, where $\tilde{h}_{\mathbf{10}}^u = i\sigma_2(h_{\mathbf{10}}^u)^*$. These field decompositions introduce particles beyond the SM spectrum and may contribute to the renormalisation group running behaviour of the gauge coefficients. However, we reduce their redundancy in the following way: For scale Q which varies in the range $M_X > Q > M_3$, where G_3 is preserved, the two decomposed $(\mathbf{1}, \mathbf{2}, \mathbf{2})$'s can mix

$SO(10)$	10	$\overline{\mathbf{126}}$	120
G_3	$(\mathbf{1}, \mathbf{2}, \mathbf{2})_1$	$(\mathbf{15}, \mathbf{2}, \mathbf{2})_1$ $+(\mathbf{10}, \mathbf{1}, \mathbf{3}) + (\overline{\mathbf{10}}, \mathbf{3}, \mathbf{1})$	$(\mathbf{1}, \mathbf{2}, \mathbf{2})_2 + (\mathbf{15}, \mathbf{2}, \mathbf{2})_2$
G_2	$(\mathbf{1}, \mathbf{2}, \mathbf{2}, 0)_1$	$(\mathbf{1}, \mathbf{2}, \mathbf{2}, 0)_2$ $+(\mathbf{1}, \mathbf{1}, \mathbf{3}, -1) + (\mathbf{1}, \mathbf{3}, \mathbf{1}, 1)$	$(\mathbf{1}, \mathbf{2}, \mathbf{2}, 0)_{3,4}$
G_1	$(\mathbf{1}, \mathbf{2}, \mathbf{2}, 0)_1$	$(\mathbf{1}, \mathbf{2}, \mathbf{2}, 0)_2$ $+(\mathbf{1}, \mathbf{1}, \mathbf{3}, -1)$	$(\mathbf{1}, \mathbf{2}, \mathbf{2}, 0)_{3,4}$
G_{SM}	$(\mathbf{1}, \mathbf{2}, -1/2)_{h_{\mathbf{10}}^u}$ $+(\mathbf{1}, \mathbf{2}, +1/2)_{h_{\mathbf{10}}^d}$	$(\mathbf{1}, \mathbf{2}, -1/2)_{h_{\overline{\mathbf{126}}}^u}$ $+(\mathbf{1}, \mathbf{2}, +1/2)_{h_{\overline{\mathbf{126}}}^d}$ $+(\mathbf{1}, \mathbf{1}, 0)_S$	$(\mathbf{1}, \mathbf{2}, -1/2)_{h_{\mathbf{120}}^u, h_{\mathbf{120}}^{u'}}$ $+(\mathbf{1}, \mathbf{2}, +1/2)_{h_{\mathbf{120}}^d, h_{\mathbf{120}}^{d'}}$

Table 4: Decomposition of Higgses responsible for the fermion mass generation. $\overline{\mathbf{126}}$ is the same Higgs as shown in Table 2 and it is responsible for both the breaking $G_1 \rightarrow G_{\text{SM}}$ and right-handed neutrino mass generation. $(\mathbf{1}, \mathbf{1}, 0)_S$ is the same singlet given in Table 2.

and we assume that the heavy one gains a mass $\sim M_X$ and thus decouples at scales below M_X . The same assumption applies to the other two $(\mathbf{1}, \mathbf{2}, \mathbf{2})$'s. Using these assumptions, we have two bi-doublets $(\mathbf{1}, \mathbf{2}, \mathbf{2}, 0)$ at the scale $M_3 > Q > M_2$ and $M_2 > Q > M_1$, where G_2 and G_1 are preserved, respectively. We retain them as the physically relevant degrees of freedom in this range of scales, following the logic of Ref. [12]. Four electroweak doublets remain at energies below M_1 but above the electroweak scale. Naively, one can assume all massive states are sufficiently heavy that they decouple at scale M_1 , except for the lightest electroweak doublet, which is the SM Higgs and should be massless before electroweak symmetry breaking. Without loss of generality, we can write these Higgses as superpositions of mass eigenstates, $\hat{h}_i = \sum_j V_{ij} h_j$, with $h_{\text{SM}} \equiv \hat{h}_1$, where V is a unitary matrix and the heavy doublets that decouple at M_X have also been taken into account. With this treatment, all physical degrees of freedom present at the relevant scale are the same as those of chain III4 in Ref. [12]. For the second Higgs multiplet, $\overline{\mathbf{126}}$, we retain another decomposed representation $(\mathbf{10}, \mathbf{3}, \mathbf{1})$ of G_1 , which contains a $SU(2)_L$ triplet, $(\mathbf{1}, \mathbf{1}, \mathbf{3}, -1)$, of G_2 and G_1 which contains the singlet $S \sim (\mathbf{1}, \mathbf{1}, 0)$ of G_{SM} that is important not only in its role in symmetry breaking, but also in the generation of neutrino masses. $(\overline{\mathbf{10}}, \mathbf{3}, \mathbf{1})$ is retained due to the requirement of left-right parity symmetry, Z_2^C , and it is decomposed to a $(\mathbf{1}, \mathbf{3}, \mathbf{1}, 1)$ of G_2 . After G_2 breaking, i.e., the breaking of the left-right parity symmetry, we assume that this particle decouples.

In the Yukawa sector, couplings above the GUT scale are given by

$$Y_{\mathbf{10}}^* \mathbf{16} \cdot \mathbf{16} \cdot \mathbf{10} + Y_{\overline{\mathbf{126}}}^* \mathbf{16} \cdot \mathbf{16} \cdot \overline{\mathbf{126}} + Y_{\mathbf{120}}^* \mathbf{16} \cdot \mathbf{16} \cdot \mathbf{120} + \text{h.c.}, \quad (2.2)$$

where the asterisk denotes complex conjugation. Considering the flavour indices, $Y_{\mathbf{10}}$ and $Y_{\overline{\mathbf{126}}}$ are in general complex 3×3 symmetric matrices and $Y_{\mathbf{120}}$ is an antisymmetric matrix. In the non-SUSY case, two further couplings $\mathbf{16} \cdot \mathbf{16} \cdot \mathbf{10}^*$ and $\mathbf{16} \cdot \mathbf{16} \cdot \mathbf{120}^*$ are allowed

by the gauge symmetry; however, we forbid them by imposing an additional Peccei–Quinn $U(1)$ symmetry [22] as described in [23–25]. After the final symmetry is broken to G_{SM} , the above Yukawa terms generate the following SM fermion mass terms in the left-right convention:

$$\begin{aligned}
& Y_{\mathbf{10}} \left[(\bar{Q}u_R + \bar{L}\nu_R)h_{\mathbf{10}}^u + (\bar{Q}d_R + \bar{L}e_R)h_{\mathbf{10}}^d \right] + \frac{1}{\sqrt{3}}Y_{\mathbf{126}} \left[(\bar{Q}u_R - 3\bar{L}\nu_R)h_{\mathbf{126}}^u + (\bar{Q}d_R - 3\bar{L}e_R)h_{\mathbf{126}}^d \right] \\
& + Y_{\mathbf{120}} \left[(\bar{Q}u_R + \bar{L}\nu_R)h_{\mathbf{120}}^u + (\bar{Q}d_R + \bar{L}e_R)h_{\mathbf{120}}^d + \frac{1}{\sqrt{3}}(\bar{Q}u_R - 3\bar{L}\nu_R)h_{\mathbf{120}}^{u'} + (\bar{Q}d_R - 3\bar{L}e_R)h_{\mathbf{120}}^{d'} \right] + \text{h.c.}
\end{aligned} \tag{2.3}$$

Rotating the Higgs fields to their mass basis, we derive Yukawa couplings to the SM Higgs as

$$Y_u \bar{Q} \tilde{h}_{\text{SM}} u_R + Y_d \bar{Q} h_{\text{SM}} d_R + Y_\nu \bar{L} \tilde{h}_{\text{SM}} \nu_R + Y_e \bar{L} h_{\text{SM}} e_R + \text{h.c.}, \tag{2.4}$$

where

$$\begin{aligned}
Y_u &= Y_{\mathbf{10}} V_{11}^* + \frac{1}{\sqrt{3}} Y_{\mathbf{126}} V_{12}^* + Y_{\mathbf{120}} \left(V_{13}^* + \frac{1}{\sqrt{3}} V_{14}^* \right), \\
Y_d &= Y_{\mathbf{10}} V_{15} + \frac{1}{\sqrt{3}} Y_{\mathbf{126}} V_{16} + Y_{\mathbf{120}} \left(V_{17} + \frac{1}{\sqrt{3}} V_{18} \right), \\
Y_\nu &= Y_{\mathbf{10}} V_{11}^* - \sqrt{3} Y_{\mathbf{126}} V_{12}^* + Y_{\mathbf{120}} \left(V_{13}^* - \sqrt{3} V_{14}^* \right), \\
Y_e &= Y_{\mathbf{10}} V_{15} - \sqrt{3} Y_{\mathbf{126}} V_{16} + Y_{\mathbf{120}} \left(V_{17} - \sqrt{3} V_{18} \right).
\end{aligned} \tag{2.5}$$

A Majorana mass term for the right-handed neutrinos is generated from the second term of Eq. (2.2):

$$Y_{\mathbf{126}} \bar{\nu}_R \phi_S \nu_R^c + \text{h.c.}, \tag{2.6}$$

once ϕ_S acquires a VEV, v_S , which controls the scale of the masses:

$$M_{\nu_R} = Y_{\mathbf{126}} v_S. \tag{2.7}$$

After the right-handed neutrinos decouple and electroweak symmetry is broken, the light neutrinos acquire their mass via the Type-I seesaw mechanism [26–29]:

$$M_\nu = -Y_\nu M_{\nu_R}^{-1} Y_\nu^T v_{\text{SM}}^2, \tag{2.8}$$

where the SM Higgs VEV is $v_{\text{SM}} = 175$ GeV. We emphasise that the electroweak singlet, ϕ_S , is essential for the symmetry breaking $G_1 \rightarrow G_{\text{SM}}$ and thus, its VEV determines the scale of M_1 and the right-handed neutrino masses. As required by perturbativity, $Y_{\mathbf{126}} \lesssim \mathcal{O}(1)$, the mass of the heaviest right-handed neutrino, M_{N_3} , should be not heavier than the lowest intermediate scale, M_1 . On the other hand, neutrino oscillation experiments have given relatively precise measurements of light neutrino masses and mixing angles. These data restrict the right-handed neutrino mass spectrum via the seesaw formula, and a realistic GUT model should survive all such constraints.

2.3 Gauge Unification

Given an arbitrary gauge symmetry G , which can be expressed as a product of simple Lie groups, $G = H_1 \times \cdots \times H_n$, the two-loop renormalisation group running equation for group H_i , for $i = 1, 2, \dots$, is given by

$$Q \frac{d\alpha_i}{dQ} = \beta_i(\alpha_i), \quad (2.9)$$

where $\alpha_i = g_i^2/(4\pi)$ and the β function is determined by the particle content of the theory:

$$\beta_i = -\frac{1}{2\pi} \alpha_i^2 (b_i + \frac{1}{4\pi} \sum_j b_{ij} \alpha_j). \quad (2.10)$$

Here, $i \in [1, \dots, n]$ for H_n , g_i is the gauge coefficient of H_i , and b_i and b_{ij} refer to the normalised coefficients of one- and two-loop contributions, respectively. In the following, we neglect the Yukawa contribution to the RG running equations as it gives a subdominant contribution. Given two scales Q_0 and Q , if the conditions $Q_0 < Q$ and $b_j \alpha_j(Q_0) \log(Q/Q_0) < 1$ are both satisfied then an analytical solution for these equations can be obtained [30]:

$$\alpha_i^{-1}(Q) = \alpha_i^{-1}(Q_0) - \frac{b_i}{2\pi} \log \frac{Q}{Q_0} + \sum_j \frac{b_{ij}}{4\pi b_i} \log \left(1 - \frac{b_j}{2\pi} \alpha_j(Q_0) \log \frac{Q}{Q_0} \right). \quad (2.11)$$

In the case that both H_i and H_j are non-abelian groups, the coefficients b_i and b_{ij} are

$$\begin{aligned} b_i &= -\frac{11}{3} C_2(H_i) + \frac{2}{3} \sum_F T(\psi_i) + \frac{1}{3} \sum_S T(\phi_i), \\ b_{ij} &= -\frac{34}{3} [C_2(H_i)]^2 \delta_{ij} + \sum_F T(\psi_i) [2C_2(\psi_j) + \frac{10}{3} C_2(H_i) \delta_{ij}] \\ &\quad + \sum_S T(\phi_i) [4C_2(\phi_j) + \frac{2}{3} C_2(H_i) \delta_{ij}], \end{aligned} \quad (2.12)$$

where the ψ and ϕ indices sum over the fermions and complex scalar multiplets, respectively, and ψ_i and ϕ_i are their representations in the group H_i , respectively. $C_2(R_i)$ (for $R_i = \psi_i, \phi_i$) denotes the quadratic Casimir of the representation R_i in group H_i and $C_2(H_i)$ is the quadratic Casimir of the adjoint presentation of the group H_i .

In particular, for $SU(N)$, $C_2(SU(N)) = N$ and the quadratic Casimir of the fundamental irrep \mathbf{N} of $SU(N)$ is given by $C_2(\mathbf{N}) = (N^2 - 1)/2N$; for $SO(10)$, $C_2(SO(10)) = 8$, and the quadratic Casimir of the fundamental irrep $\mathbf{10}$ of $SO(10)$ is given by $C_2(\mathbf{10}) = 9/2$. The spinor representation of $SO(10)$, $\mathbf{16}$, has $C_2(\mathbf{16}) = 45/4$. $T(R_i)$ is the Dynkin index of representation R_i of group H_i . For $SU(N)$, $T(R_i) = C_2(R_i) d(R_i)/(N^2 - 1)$ where $d(R_i)$ is the dimension of R_i . If one of H_j is a $U(1)$ symmetry, the coefficient b_{ij} is obtained by replacing $C_2(R_j)$ and $T(R_j)$ with the charge square $[Q_j(R)]^2$ of the field multiplet R in $U(1)_j$. For the Abelian symmetry, $C_2(U(1)) = 0$.

Explicit values of b_i and b_{ij} depend on the degree of freedoms introduced by the gauge, matter and Higgs fields. The gauge fields are directly determined by the gauge symmetry

in the breaking chain. In regards to the matter fields, we assume they are the minimal extension which includes all the SM fermions, i.e., minimally a $\mathbf{16}$ of $SO(10)$ as in Table 3. The most significant uncertainty contributing to RG running comes from the Higgs sector as one has to account for all the Higgses used to generate fermion masses and the GUT and intermediate symmetry breaking. Given the decomposition of Higgs fields in Table 2 and the discussion in Section 2.2, the Higgs fields included in each step of the RG running are:

- For $G_1 \rightarrow G_{\text{SM}}$, we include only the SM Higgs. Although we arrive at a series of electroweak doublets after field decomposition, we assume that all degrees of freedom except the SM Higgs are sufficiently heavy that they are integrated out by this breaking step and thus have a negligible effect on the RG running.
- For $G_2 \rightarrow G_1$, we include three Higgses in the running, two $(\mathbf{1}, \mathbf{2}, \mathbf{2}, 0)$'s and one $(\mathbf{1}, \mathbf{1}, \mathbf{3}, -1)$ of G_1 . The former includes the SM Higgs, and the latter includes the gauge singlet ϕ_S of G_{SM} which is used to achieve the breaking of $G_1 \rightarrow G_{\text{SM}}$ and right-handed neutrino masses.
- For $G_3 \rightarrow G_2$, we include two $(\mathbf{1}, \mathbf{2}, \mathbf{2}, 0)$'s, $(\mathbf{1}, \mathbf{1}, \mathbf{3}, -1)$, $(\mathbf{1}, \mathbf{3}, \mathbf{1}, 1)$, and $(\mathbf{1}, \mathbf{1}, \mathbf{1}, 0)_2$ in the RG running. Two further Higgses are included compared to the above item as $(\mathbf{1}, \mathbf{3}, \mathbf{1}, 1)$ is required for the matter parity symmetry Z_2^C and $(\mathbf{1}, \mathbf{1}, \mathbf{1}, 0)_2$ is used to break Z_2^C , $G_2 \rightarrow G_1$.
- For $SO(10) \rightarrow G_3$, we include $(\mathbf{1}, \mathbf{2}, \mathbf{2})$, $(\mathbf{15}, \mathbf{2}, \mathbf{2})$, $(\mathbf{10}, \mathbf{1}, \mathbf{3})$, $(\overline{\mathbf{10}}, \mathbf{3}, \mathbf{1})$ and two $(\mathbf{15}, \mathbf{1}, \mathbf{1})$'s in the RG running. The former two are required to obtain the two $(\mathbf{1}, \mathbf{2}, \mathbf{2}, 0)$'s above. $(\mathbf{10}, \mathbf{1}, \mathbf{3})$ and $(\overline{\mathbf{10}}, \mathbf{3}, \mathbf{1})$ are required for $(\mathbf{1}, \mathbf{1}, \mathbf{3}, -1)$ and $(\mathbf{1}, \mathbf{3}, \mathbf{1}, 1)$. One $(\mathbf{15}, \mathbf{1}, \mathbf{1})$, decomposed from $\mathbf{45}$ is for $(\mathbf{1}, \mathbf{1}, \mathbf{1}, 0)_2$, and the other, decomposed from $\mathbf{210}$, includes the singlet $(\mathbf{1}, \mathbf{1}, \mathbf{1}, 0)_1$ to achieve the breaking $G_3 \rightarrow G_2$.

By including the above particle content in the RG running, we obtain the coefficients b_i and b_{ij} at the two-loop level, which we list in Table 5 and are the same as in the chain III4 of Ref. [12]. Although we include one more Higgs multiplet $\mathbf{120}$, the contribution of induced new particles can be ignored, as explained in the previous subsection, by assuming heavy mass eigenstates heavier than the breaking scale, M_X [31]. In order to keep the treatment of the RG running economical, the scalar multiplets which are unnecessary for the breaking chain are assumed to be as massive as the $SO(10)$ breaking scale M_X . Therefore, these scalars will not affect the RG running or provide threshold corrections.

During the symmetry breaking at an intermediate scale (M_3 , M_2 or M_1), gauge couplings of the larger symmetry and those of the residual symmetry after spontaneous symmetry breaking (SSB) must satisfy matching conditions. Here we list one-loop matching conditions that appear in the GUT breaking chains. For a simple Lie group H_{i+1} broken to subgroup H_i at the scale $Q = M_I$, the one-loop matching condition is given by [32]

$$H_{i+1} \rightarrow H_i : \quad \alpha_{H_{i+1}}^{-1}(M_I) - \frac{1}{12\pi} C_2(H_{i+1}) = \alpha_{H_i}^{-1}(M_I) - \frac{1}{12\pi} C_2(H_i). \quad (2.13)$$

$SO(10)$	broken at $Q = M_X$	
↓	$\{b_i\} = \begin{pmatrix} \frac{10}{3} \\ \frac{26}{3} \\ \frac{26}{3} \end{pmatrix}$,	$\{b_{ij}\} = \begin{pmatrix} \frac{4447}{2} & \frac{249}{2} & \frac{249}{2} \\ \frac{1245}{2} & \frac{779}{3} & 48 \\ \frac{1245}{2} & 48 & \frac{779}{3} \end{pmatrix}$
G_3	broken at $Q = M_3$	
↓	$\{b_i\} = \begin{pmatrix} -7 \\ -2 \\ -2 \\ 7 \end{pmatrix}$,	$\{b_{ij}\} = \begin{pmatrix} -26 & \frac{9}{2} & \frac{9}{2} & \frac{1}{2} \\ 12 & 31 & 6 & \frac{27}{2} \\ 12 & 6 & 31 & \frac{27}{2} \\ 4 & \frac{81}{2} & \frac{81}{2} & \frac{115}{2} \end{pmatrix}$
G_2	broken at $Q = M_2$	
↓	$\{b_i\} = \begin{pmatrix} -7 \\ -\frac{8}{3} \\ -2 \\ \frac{11}{2} \end{pmatrix}$,	$\{b_{ij}\} = \begin{pmatrix} -26 & \frac{9}{2} & \frac{9}{2} & \frac{1}{2} \\ 12 & \frac{37}{3} & 6 & \frac{3}{2} \\ 12 & 6 & 31 & \frac{27}{2} \\ 4 & \frac{9}{2} & \frac{81}{2} & \frac{61}{2} \end{pmatrix}$
G_1	broken at $Q = M_1$	
↓	$\{b_i\} = \begin{pmatrix} -7 \\ -\frac{19}{6} \\ \frac{41}{10} \end{pmatrix}$,	$\{b_{ij}\} = \begin{pmatrix} -26 & \frac{9}{2} & \frac{11}{10} \\ 12 & \frac{35}{6} & \frac{9}{10} \\ \frac{44}{5} & \frac{17}{10} & \frac{199}{50} \end{pmatrix}$
G_{SM}		

Table 5: Coefficients b_i and b_{ij} of gauge coupling β functions appearing in the specified breaking chain.

For $G_1 \rightarrow G_{\text{SM}}$, we encounter the breaking, $SU(2)_R \times U(1)_X \rightarrow U(1)_Y$, which has the matching condition [33]:

$$SU(2)_R \times U(1)_X \rightarrow U(1)_Y : \frac{3}{5} \left(\alpha_{2R}^{-1}(M_I) - \frac{1}{6\pi} \right) + \frac{2}{5} \alpha_{1X}^{-1}(M_I) = \alpha_{1Y}^{-1}(M_I). \quad (2.14)$$

Applying the matching conditions of the above two equations, all gauge couplings of the subgroups unify into a single gauge coupling, $\alpha_X \equiv g_X^2/4\pi$, of $SO(10)$ at the GUT scale, M_X . This condition restricts both the GUT and intermediate scales for each breaking chain. We denote the mass of the heavy gauge boson masses associated with $SO(10)$ breaking as M_X and M_3 , M_2 and M_1 are associated to the breaking of G_3 , G_2 and G_1 , respectively. Correlations among M_1 , M_2 , M_3 and M_X are determined numerically using the following procedure for the breaking chain $SO(10) \rightarrow G_3 \rightarrow G_2 \rightarrow G_1 \rightarrow G_{\text{SM}}$ where the two-loop RG running evolution is performed in reverse, $G_{\text{SM}} \rightarrow G_1 \rightarrow G_2 \rightarrow G_3 \rightarrow SO(10)$:

1. Begin the evaluation from the scale M_Z with the SM gauge couplings $\alpha_3 = 0.1184$, $\alpha_2 = 0.033819$ and $\alpha_1 = 0.010168$ [34]. Evolve these couplings using the RGE of the SM to scale M_1 , where G_1 is recovered. Apply the matching conditions for the SM

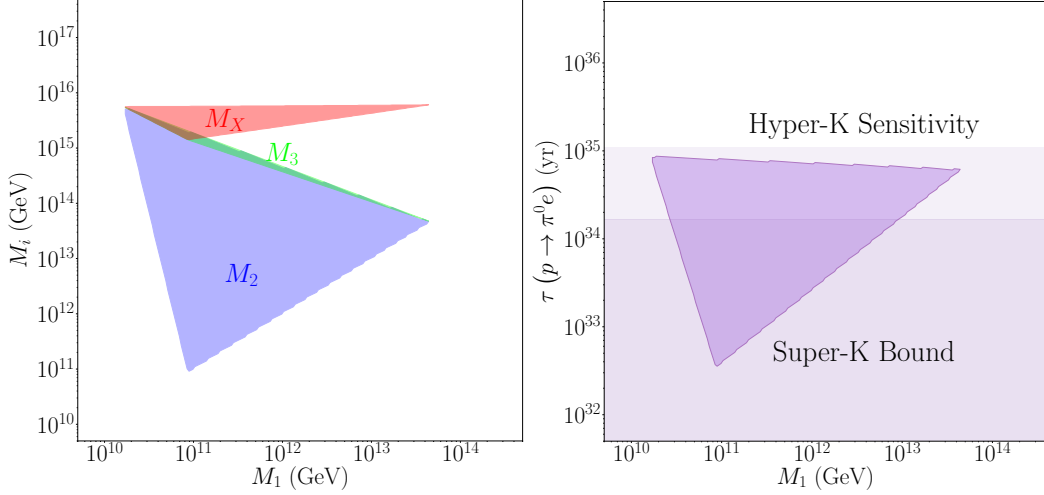


Figure 1: Left panel: regions of M_2 , M_3 , M_X as functions of M_1 allowed by gauge unification; Right panel: prediction of proton lifetime as functions of M_1 , with exclusion upper bound of Super-K and future sensitivity of Hyper-K indicated.

gauge couplings and the G_1 gauge couplings to obtain the values of couplings in the intermediate symmetry group.

2. RG evolve the G_1 gauge couplings from the scale M_1 to M_2 , where G_2 is recovered, and the gauge couplings of G_2 are obtained via matching conditions at scale M_2 .
3. Repeating this same procedure, to evolve all couplings to the GUT scale, M_X , to unify to a single value α_X with the matching condition at M_X fully accounted for.

The above RG running procedure involves four scales M_1 , M_2 , M_3 and M_X . Gauge unification requires that three SM gauge couplings meet each other at the GUT scale, up to matching conditions, and enforces two constraints; thus, there are only two free scales. The remaining scales and the gauge coupling, α_X , are then determined via gauge unification. General restrictions on the parameter space of scales i.e., M_2 , M_3 and M_X varying with M_1 , are shown in the left plot of Fig. 1.

Given the gauge unification scale, M_X , and its gauge coupling at that scale, the proton lifetime via the decaying process $p \rightarrow \pi^0 e^+$ is predicted. Due to the scale correlations imposed by gauge unification, the correlation between the proton lifetime, τ_p , and M_X can be transformed into a correlation between τ_p and any intermediate scale. Following the formulation of Ref. [12], we derive the allowed parameter space of τ_p versus intermediate scales. By varying the lowest intermediate scale M_1 , we obtain general regions of τ_p . The bound of τ_p versus the lowest scale M_1 is shown in the right panel of Fig. 1. The Super-K experiment set a lower bound on the proton lifetime, $\tau(p \rightarrow e^+ \pi^0) > 2.4 \times 10^{34}$ years at 90 % confidence level [13]. In the future, Hyper-Kamiokande (Hyper-K) is expected to improve the measurement of proton lifetime by almost one order of magnitude [20]. If proton decay is not observed, the entire parameter space of this breaking chain will be excluded.

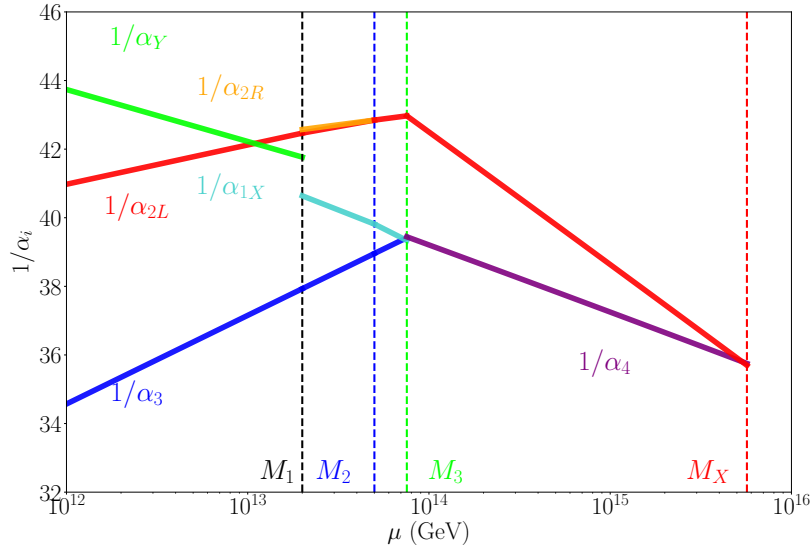


Figure 2: The RG running of gauge couplings in the breaking chain $SO(10) \rightarrow G_3 \rightarrow G_2 \rightarrow G_1 \rightarrow G_{\text{SM}}$. BP1 with the first and second lowest intermediate scales are fixed at $M_1 = 2 \times 10^{13}$ GeV and $M_2 = 5 \times 10^{13}$ GeV, the remaining scales M_3 and M_X , as well as gauge couplings α_{2R} , are determined by the gauge unification at M_X .

Benchmark Point 1 (BP1) In Fig. 2, we show an example of the RG running of the gauge couplings along with the scale and fix

$$M_1 = 2 \times 10^{13} \text{ GeV}, \quad M_2 = 5 \times 10^{13} \text{ GeV}, \quad (2.15)$$

where the remaining scales, M_3 and M_X , as well as the gauge coupling α_X , are then determined via the gauge unification,

$$M_3 = 7.55 \times 10^{13} \text{ GeV}, \quad M_X = 5.68 \times 10^{15} \text{ GeV}, \quad \alpha_X = 0.0279. \quad (2.16)$$

This benchmark point will be considered throughout this paper. Its associated proton decay rate, $\tau(p \rightarrow e^+\pi^0) \sim 5.1 \times 10^{34}$ years, is consistent with the current Super-K bound and will be tested by Hyper-K. We note that BP1 is consistent with SM fermion masses and mixing to a high statistical significance, and this requires $M_1 \sim 10^{13}$ GeV. Such a high value for M_1 leads a compressed hierarchy between M_1 , M_2 and M_3 and this comes from the constraint of gauge unification (from the left panel of Fig. 1 this region is in the right corner of the blue triangle.)

3 Fermion masses and mixing

As all the SM fermions are embedded in the same $SO(10)$ multiplet (16), their masses are correlated with each other. Therefore, it is a non-trivial task to find regions of the GUT model parameter space that predict the SM fermion masses and mixing consistent with the precisely measured (particularly in the quark sector) experimental data. This

section presents the correlations of masses and mixing between quarks and leptons and predicts heavy neutrino masses using the model we discussed in the previous section. We parametrise the up, down, neutrino, charged lepton Yukawa couplings and right-handed neutrino mass matrix, respectively, as follows [35]:

$$\begin{aligned} Y_u &= h + r_2 f + i r_3 h', & Y_d &= r_1 (h + f + i h'), & Y_\nu &= h - 3r_2 f + i c_\nu h', \\ Y_e &= r_1 (h - 3f + i c_e h'), & M_{\nu R} &= f \frac{\sqrt{3} r_1}{V_{16}} v_S, \end{aligned} \quad (3.1)$$

where

$$\begin{aligned} h &= Y_{\mathbf{10}} V_{11}, \quad f = Y_{\overline{\mathbf{126}}} \frac{V_{16} V_{11}^*}{\sqrt{3} V_{15}}, \quad c_e = \frac{V_{17} - \sqrt{3} V_{18}}{V_{17} + V_{18}/\sqrt{3}}, \quad c_\nu = \frac{V_{13} - \sqrt{3} V_{14}}{V_{17} + V_{18}/\sqrt{3}} \frac{V_{15}}{V_{11}^*}, \\ r_1 &= \frac{V_{15}}{V_{11}^*}, \quad r_2 = \frac{V_{12}^* V_{15}}{V_{16} V_{11}^*}, \quad r_3 = \frac{V_{13}^* + V_{14}^*/\sqrt{3} V_{15}}{V_{17} + V_{18}/\sqrt{3} V_{11}^*}, \quad h' = -i Y_{\mathbf{120}} \left(V_{17} + V_{18}/\sqrt{3} \right) \frac{V_{11}^*}{V_{15}}, \end{aligned} \quad (3.2)$$

and V_{ji} denotes the mixing between the mass and interaction basis of the electroweak Higgs doublets. The light neutrino mass matrix, M_ν , is obtained by

$$M_\nu = m_0 Y_\nu f^{-1} Y_\nu, \quad (3.3)$$

where $m_0 = -\frac{V_{16}}{\sqrt{3} r_1} \frac{v_{\text{SM}}^2}{v_S}$.

3.1 Parametrisation using Hermitian Yukawa matrices

The most general form of Yukawa couplings and neutrino mass matrix includes many free parameters. A considerable reduction in the number of parameters can be achieved by considering only the Hermitian case for all fermion Yukawa couplings matrices Y_u , Y_d , Y_ν and Y_e (and M_R should be real as a consequence of the Majorana nature for right-handed neutrinos). Such a reduction can result from spontaneous CP violation [36, 37] which assumes that there exists a CP symmetry above the GUT scale, leading to real-valued $Y_{\mathbf{10}}$, $Y_{\overline{\mathbf{126}}}$ and $Y_{\mathbf{120}}$, and the CP is broken by some complex VEVs of Higgs multiplets during GUT or intermediate symmetry breaking. For the particular chain we applied in the last section, one can consider, for example, the parity-odd singlet of $G_2 \equiv SU(3)_c \times SU(2)_L \times SU(2)_R \times U(1)_X \times Z_2^C$, decomposed from $\mathbf{45}$, gains a purely imaginary VEV. Then, via couplings such as $\mathbf{45} \cdot \mathbf{10} \cdot \mathbf{120}$ (and $\mathbf{45} \cdot \overline{\mathbf{126}} \cdot \mathbf{120}$) which generate purely imaginary off-diagonal mass terms between $h_{\mathbf{10}}^{u,d}$ and $h_{\mathbf{120}}^{u,d}$ (and those between $h_{\overline{\mathbf{126}}}^{u,d}$ and $h_{\mathbf{120}}^{u,d}$) and further purely imaginary mixing entries V_{13} , V_{14} (and V_{17} , V_{18}) are obtained. As a result, h , f and h' , as well as all parameters on the right-hand side of Eq. (3.1), are real. Since h' is antisymmetric, we arrive at Hermitian Dirac Yukawa coupling matrices Y_u , Y_d , Y_ν and Y_e . This texture has widely been applied in the literature, see e.g., Refs. [23, 31, 38]. The resulting fermion mass matrices conserve parity symmetry $L \leftrightarrow R$ [31] and following from the assumption that there is no CP violation in the Higgs sector, apart from that of $\mathbf{120}$, r_1 , r_2 , r_3 , c_e , and c_ν are all real parameters resulting in a real symmetric right-handed

neutrino mass matrix, $M_{\nu R}$. The CP symmetry in the Yukawa coupling is spontaneously broken after the Higgses gain VEVs.

For simplicity, we assume that $r_3 = 0$, which implies that the imaginary part of Y_u vanishes. It is convenient to write the up-type Yukawa in the diagonal basis

$$Y_u = h + r_2 f = \text{diag}\{\eta_u y_u, \eta_c y_c, \eta_t y_t\}, \quad (3.4)$$

which can be achieved via a real-orthogonal transformation on the fermion flavours without changing the Hermitian property of Y_d , Y_e , and Y_ν . In the above, $\eta_{u,c,t} = \pm 1$ refer to signs that cannot be determined by the real-orthogonal transformation. While $\eta_t = +1$ can be fixed by making an overall sign rotation for all Yukawa matrices, the remaining signs, η_u and η_c , cannot be fixed and are randomly varied throughout our analysis. In the basis of the diagonal up-quark mass matrix, Y_d is given by

$$Y_d = P_a V_{\text{CKM}} \text{diag}\{\eta_d y_d, \eta_s y_s, \eta_b y_b\} V_{\text{CKM}}^\dagger P_a^*, \quad (3.5)$$

where again $\eta_{d,s,b} = \pm 1$ represent the signs of eigenvalues, and V_{CKM} is the CKM matrix parametrised in the following form

$$V_{\text{CKM}} = \begin{pmatrix} c_{12}c_{13} & s_{12}c_{13} & s_{13}e^{-i\delta_q} \\ -s_{12}c_{23} - c_{12}s_{13}s_{23}e^{i\delta_q} & c_{12}c_{23} - s_{12}s_{13}s_{23}e^{i\delta_q} & c_{13}s_{23} \\ s_{12}s_{23} - c_{12}s_{13}c_{23}e^{i\delta_q} & -c_{12}s_{23} - s_{12}s_{13}c_{23}e^{i\delta_q} & c_{13}c_{23} \end{pmatrix}, \quad (3.6)$$

where $s_{ij} = \sin \theta_{ij}^q$, $c_{ij} = \cos \theta_{ij}^q$ and $P_a = \text{diag}\{e^{ia_1}, e^{ia_2}, 1\}$. The matrices h , f and h' are then expressed in terms of Y_u and Y_d

$$h = -\frac{Y_u}{r_2 - 1} + \frac{r_2 \text{Re}Y_d}{r_1(r_2 - 1)}, \quad f = \frac{Y_u}{r_2 - 1} - \frac{\text{Re}Y_d}{r_1(r_2 - 1)}, \quad h' = i \frac{\text{Im}Y_d}{r_1},$$

where Y_ν , Y_e are

$$\begin{aligned} Y_\nu &= -\frac{3r_2 + 1}{r_2 - 1} Y_u + \frac{4r_2}{r_1(r_2 - 1)} \text{Re}Y_d + i \frac{c_\nu}{r_1} \text{Im}Y_d, \\ Y_e &= -\frac{4r_1}{r_2 - 1} Y_u + \frac{r_2 + 3}{r_2 - 1} \text{Re}Y_d + i c_e \text{Im}Y_d. \end{aligned} \quad (3.7)$$

The light neutrino mass matrix can be expressed as

$$\begin{aligned} M_\nu &= m_0 \left(\frac{8r_2(r_2 + 1)}{r_2 - 1} Y_u - \frac{16r_2^2}{r_1(r_2 - 1)} \text{Re}Y_d \right. \\ &\quad \left. + \frac{r_2 - 1}{r_1} (r_1 Y_u + i c_\nu \text{Im}Y_d) (r_1 Y_u - \text{Re}Y_d)^{-1} (r_1 Y_u - i c_\nu \text{Im}Y_d) \right). \end{aligned} \quad (3.8)$$

Using this parametrisation, all six quark masses and four CKM mixing parameters are treated as inputs, and we are then left with seven parameters (a_1 , a_2 , r_1 , r_2 , c_e , c_ν , and m_0) to fit eight observables, including three Yukawa couplings y_e , y_μ , y_τ , two neutrino mass-squared differences Δm_{21}^2 , Δm_{31}^2 and three mixing angles θ_{12} , θ_{13} , θ_{23} , where the leptonic CP-violating phase, δ , will be treated as a prediction².

²While we do not show the Majorana phases, we compute the effective Majorana mass.

3.2 Procedure of numerical analysis

This section describes how we identify regions of our model parameter space consistent with fermion masses and mixing while evading the existing proton decay limit. In our numerical analysis, we use the following experimental data:

- We fix the Yukawa couplings (y) of charged fermions and CKM mixing angles (θ) at their best-fit (bf) values [23, 39, 40]

$$\begin{aligned} y_u^{\text{bf}} &= 2.54 \times 10^{-6}, & y_c^{\text{bf}} &= 1.37 \times 10^{-3}, & y_t^{\text{bf}} &= 0.43, \\ y_d^{\text{bf}} &= 6.56 \times 10^{-6}, & y_s^{\text{bf}} &= 1.24 \times 10^{-4}, & y_b^{\text{bf}} &= 5.7 \times 10^{-3}, \\ y_e^{\text{bf}} &= 2.70 \times 10^{-6}, & y_\mu^{\text{bf}} &= 5.71 \times 10^{-4}, & y_\tau^{\text{bf}} &= 9.7 \times 10^{-3}, \end{aligned} \quad (3.9)$$

and

$$\theta_{12}^{q,\text{bf}} = 0.227, \quad \theta_{23}^{q,\text{bf}} = 4.858 \times 10^{-2}, \quad \theta_{13}^{q,\text{bf}} = 4.202 \times 10^{-3}, \quad \delta^{q,\text{bf}} = 1.207. \quad (3.10)$$

These values are obtained by RG evolving the experimental best-fit values at a low scale to 2×10^{16} GeV, where we have ignored the experimental errors. For simplicity, small corrections induced by RG running above intermediate scales have been ignored, but their inclusion would further relax the parameter space.³ However, as we will later see, fixing them at the best fit values is sufficient to reproduce all mixing data. Thus, in this current discussion, we will ignore them for simplicity.

- In the neutrino sector, we use the best-fit values from NuFIT 5.1 [41] and include the 1σ uncertainty. Those data with and without Super-K atmospheric data are, respectively, given by

$$\begin{aligned} \Delta m_{21}^2 &= (7.42 \pm 0.21) \times 10^{-5} \text{ eV}^2, & \Delta m_{3l}^2 &= (2.510 \pm 0.027) \times 10^{-3} \text{ eV}^2, \\ \theta_{12} &= 33.45^\circ \pm 0.77^\circ, & \theta_{23} &= 42.1^\circ \pm 1.1^\circ, & \theta_{13} &= 8.62^\circ \pm 0.12^\circ, \end{aligned} \quad (3.11)$$

and

$$\begin{aligned} \Delta m_{21}^2 &= (7.42 \pm 0.21) \times 10^{-5} \text{ eV}^2, & \Delta m_{3l}^2 &= (2.514 \pm 0.028) \times 10^{-3} \text{ eV}^2, \\ \theta_{12} &= 33.44^\circ \pm 0.77^\circ, & \theta_{23} &= 49.0^\circ \pm 1.3^\circ, & \theta_{13} &= 8.57^\circ \pm 0.13^\circ, \end{aligned} \quad (3.12)$$

The atmospheric mixing angle, θ_{23} , is restricted to first octant ($0 < \theta_{23} < 45^\circ$) and the second ($45^\circ < \theta_{23} < 90^\circ$), respectively, in the two cases. In both cases, normal ordering (i.e., $m_1 < m_2 < m_3$) of neutrino masses is assumed. Inverted ordering (i.e., $m_3 < m_1 < m_2$) will not be discussed as a preliminary scan indicates that our model does not favour the inverted ordering. We do not consider the small flavour-dependent RG running effect due to the suppression of charged lepton Yukawa coupling.

³Although the coupling for the heaviest RH neutrino in Eq.(2.6) can be of order 1, its contribution to RG running is under control and is expected to be at most 5% as $M_X/M_1 \sim 10^{-2}$.

The statistical analysis is performed in the following way:

- As quark masses and mixing parameters are fixed at their best-fit values, Y_u is fully determined except for the signs of η_u and η_d (note that $\eta_t = +1$ is fixed by an overall sign rotation). Y_d depends on two free model parameters, a_1 and a_2 , and signs (η_d, η_s, η_b) .
- Based on Eq. (3.7), Y_e depends on the two phases a_1, a_2 and three ratios r_1, r_2, c_e up to the above sign differences. Note that Y_e must satisfy three equations simultaneously:

$$\begin{aligned}\text{Tr}[Y_e Y_e^\dagger] &= y_e^2 + y_\mu^2 + y_\tau^2, \\ \text{Tr}[Y_e Y_e^\dagger Y_e Y_e^\dagger] &= y_e^4 + y_\mu^4 + y_\tau^4, \\ \text{Det}[Y_e Y_e^\dagger] &= y_e^2 y_\mu^2 y_\tau^2,\end{aligned}\tag{3.13}$$

and as the right hand side is fixed, r_1, r_2 and c_e are fully determined by the phases a_1, a_2 and the signs η_q (for $q = u, c, d, s, b$). We scan the phase parameters in the range $a_1, a_2 \in [0, 2\pi]$ and vary the signs $\eta_q = \pm 1$ randomly and solve for r_1, r_2 and c_e . Then, we substitute these values into Eq. (3.7) and determine the unitary matrix V_e used in the diagonalisation $V_e^\dagger Y_e Y_e^\dagger V_e = \text{diag}\{y_e^2, y_\mu^2, y_\tau^2\}$.

- In Eq. (3.8), the neutrino mass matrix, M_ν , is determined by two further parameters c_ν and m_0 . The former determines the flavour structure and the latter the absolute mass scale, and by scanning these parameters, we determine M_ν . The diagonalisation $V_\nu^\dagger M_\nu V_\nu^* = \text{diag}\{m_1, m_2, m_3\}$ provides the neutrino mass eigenvalues and unitary matrix V_ν .
- The PMNS matrix is given by $U_{\text{PMNS}} = V_e^\dagger V_\nu$, and the three leptonic mixing angles are derived via

$$\sin \theta_{13} = |(U_{\text{PMNS}})_{e3}|, \quad \tan \theta_{12} = \left| \frac{(U_{\text{PMNS}})_{e2}}{(U_{\text{PMNS}})_{e1}} \right|, \quad \tan \theta_{23} = \left| \frac{(U_{\text{PMNS}})_{\mu 3}}{(U_{\text{PMNS}})_{\tau 3}} \right|.\tag{3.14}$$

These angles and two mass squared differences $\Delta m_{21}^2 = m_2^2 - m_1^2$ and $\Delta m_{31}^2 = m_3^2 - m_1^2$ are taken as outputs to compare with the experimental data shown in Eq. (3.11).

In summary, once the charged fermion masses and quark mixing parameters are fixed, we are left with only four free model parameters a_1, a_2, c_ν, m_0 and signs η_q :

$$\mathcal{P}_m \in \{a_1, a_2, c_\nu, m_0, \eta_q\}.\tag{3.15}$$

We scan the model parameter space, \mathcal{P}_m , to fit five observables:

$$\mathcal{O}_n \in \{\theta_{12}, \theta_{13}, \theta_{23}, \Delta m_{21}^2, \Delta m_{31}^2\}.\tag{3.16}$$

In this way, we efficiently reduce the dimensionality of the parameter space from 17 to 5 dimensions. Following the above simplified treatment, we scan two phases a_1, a_2 in the

range $[0, \pi]$. The coefficient $|c_\nu|$ is logarithmically scanned in the range $[10^{-3}, 10^3]$, and we randomly assign its \pm sign. m_0 (meV) is solved by minimising the χ^2 function, which is used as a measure of how well our model fits the data, being defined as

$$\chi^2 = \sum_n \left[\frac{\mathcal{O}_n(\mathcal{P}_m) - \mathcal{O}_n^{\text{bf}}}{\sigma_{\mathcal{O}_n}} \right]^2. \quad (3.17)$$

Given the predefined theory model parameter space, \mathcal{P}_m , and scanning in the relevant ranges of these parameters, we determine which regions fit the experimental data by setting an upper bound of χ^2 value. This procedure of the scan is divided into two steps: We first perform a preliminary scan by setting the upper bound of $\chi^2 < 100$ and then perform a subsequent scan to find the points with $\chi^2 < 10$. The results of the first scan which uses the neutrino oscillation data of Eq. (3.11) (first octant) are shown in Fig. 3. A two-dimensional subspace of a_1 - a_2 (m_0 - c_ν) is shown in the top (bottom) left panel and predictions of θ_{23} - δ (M_{N_1} - M_{N_3}) are given in the right top (bottom) panel. M_{N_1} , M_{N_2} and M_{N_3} are three right-handed neutrino masses ordered from lightest to heaviest, and they are obtained by solving the inverse of the Type-I seesaw formula:

$$M_{\nu_R} = Y_\nu^T M_\nu^{-1} Y_\nu v_{\text{SM}}^2, \quad (3.18)$$

where the mass states of ν_R , from the lightest to heaviest, are denoted as N_1 , N_2 and N_3 . We impose an upper bound by requiring $M_{N_3} \lesssim M_1$, and this is approximately equivalent to requiring that the largest eigenvalue of $Y_{\mathbf{126}} \lesssim 1$ such that the perturbativity is respected. Since the maximal value of M_1 allowed by proton decay measurements is given by 4.4×10^{13} GeV [12], viable points in the model parameter space require that

$$M_{N_3} < 4.4 \times 10^{13} \text{ GeV}. \quad (3.19)$$

Naively, by assuming the magnitude of the Dirac Yukawa coupling $Y_\nu \sim \mathcal{O}(1)$, we know from the seesaw formula that the RHN mass scale is around 10^{15} GeV. Thus, one can expect that the condition of Eq. (3.19) rules out most points. This is confirmed by the bottom-left panel Fig. 3 where most of the points predict the heaviest neutrino mass, M_{N_3} , to be heavier than 4.4×10^{13} GeV. Therefore, these points are not consistent with the requirement of gauge unification. We then perform a second more dense scan around the former points by requiring $\chi^2 < 10$ and gauge unification, e.g., the bound of the heaviest right-handed neutrino mass satisfying Eq. (3.19). The results of this scan are shown in Figs. 4 and 5, where neutrino oscillation data in Eqs. (3.11) and (3.12) are used, respectively. In both figures, scatter plots of parameters are shown in the left panel and predictions of observables are given in the right panel. In the first 2×2 grid of both figures, we arrange two-dimensional subspaces of a_1 - a_2 , m_0 - c_ν (left), and predictions θ_{23} - δ , M_{N_1} - M_{N_3} (right). We have checked that truncating the upper bound of χ^2 from 100 to 10 removes most of the points allowed in the preliminary scan. In particular, this truncation automatically removes most points which do not satisfy the gauge unification requirement,

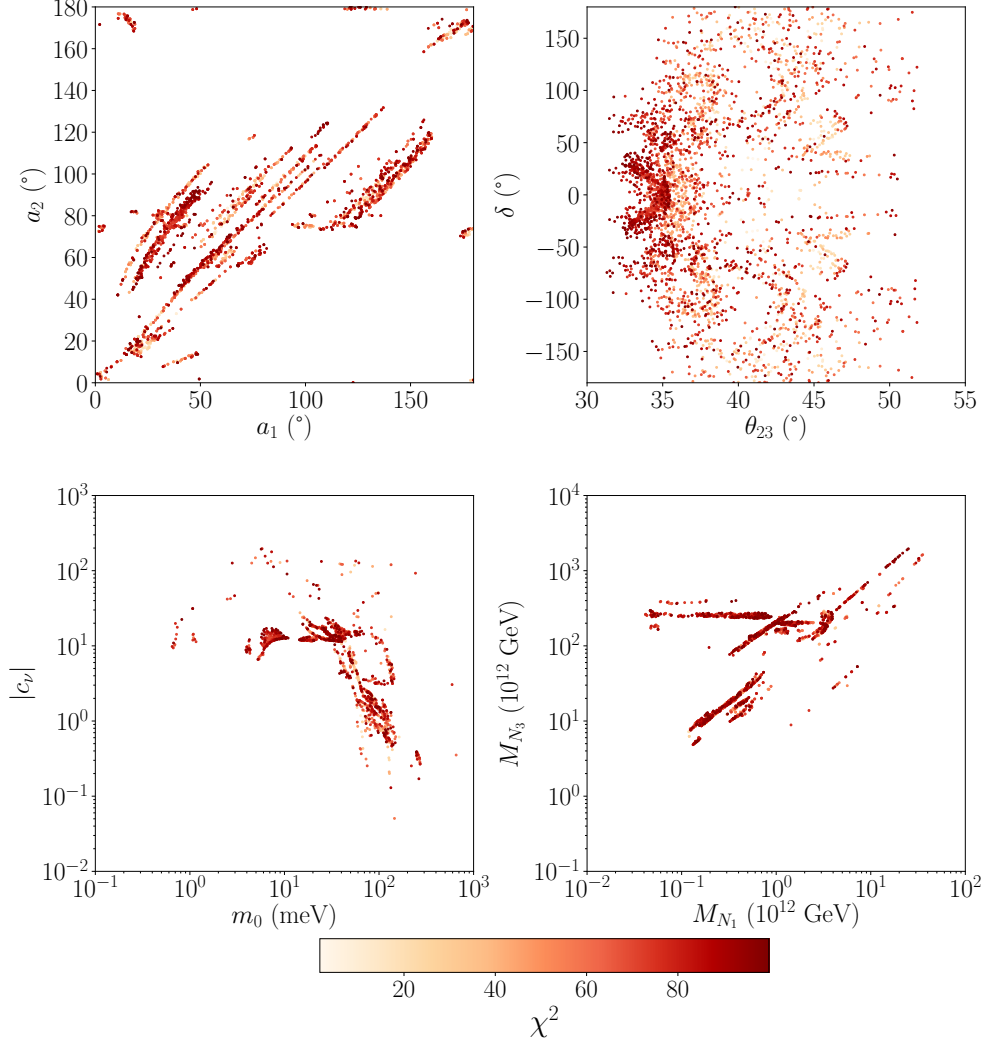


Figure 3: Two-dimensional correlations between theory inputs (left two panels) and predicted observables (right two panels) for $\chi^2 < 100$ for $\theta_{23} \leq 45^\circ$. Consistency with gauge unification is not considered.

i.e., Eq. (3.19). While only a few points are left with a large value of M_{N_3} , the gauge unification requirement fully removes them. Only a single large island of points and a few small islands nearby in the parameter space of M_{N_1} - M_{N_3} , where M_{N_3} are predicted in the range $(1, 2) \times 10^{13}$ GeV. By comparing Fig. 5 with Fig. 3, all the free parameters are strongly restricted, in particular, $a_1, a_2 \sim (50^\circ, 100^\circ)$, and $|c_\nu| \sim (1, 10)$. Notably, these points are consistent with fermion masses and mixing, gauge unification and the experimental result of proton decay measurements. In the bottom left panel of Fig. 5 we observe a linear-correlation between r_1 and r_2 which we analytically derive as follows. From experimental quark data, the following hierarchical relations exist among mixing parameters:

$$y_u : y_c : y_t \sim \theta_C^8 : \theta_C^4 : \theta_C^0,$$

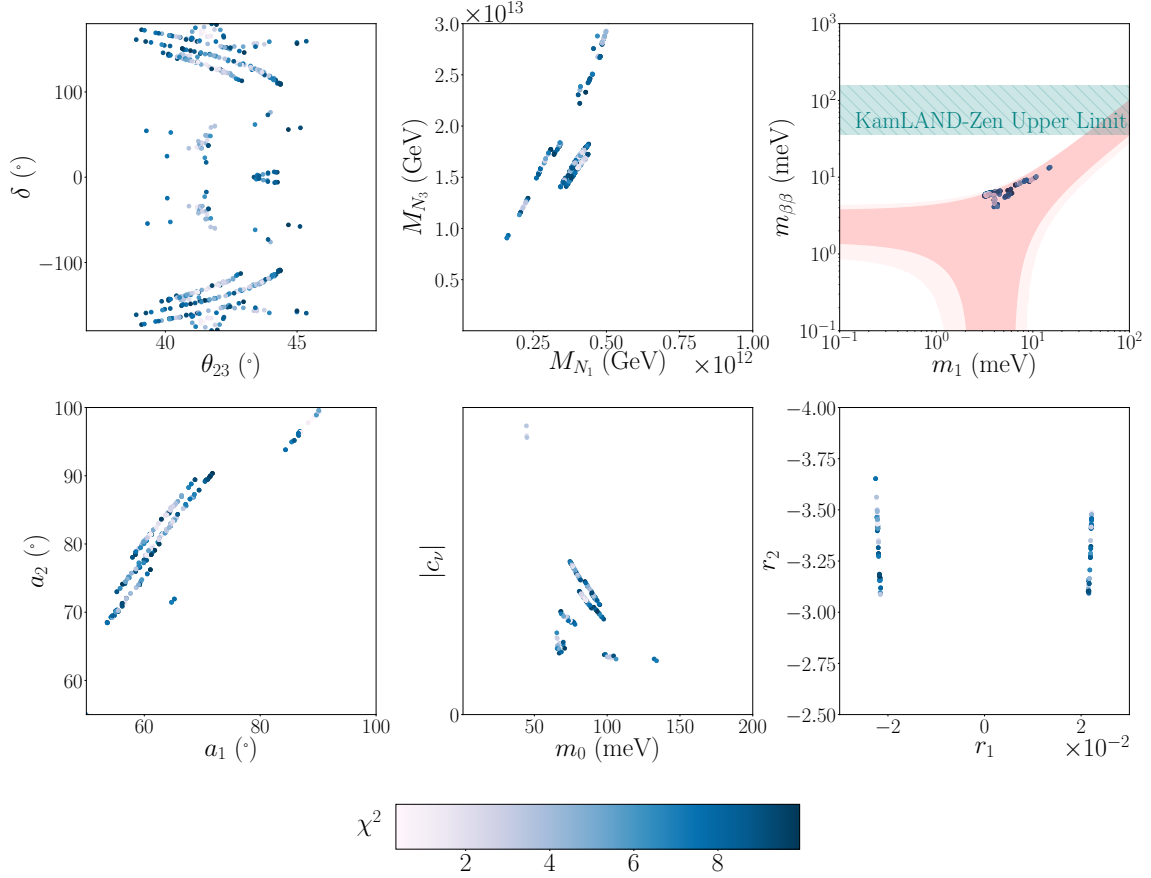


Figure 4: The predicted observables (top left two panels), the effective neutrino mass prediction (top right panel) and two-dimensional correlations between theory inputs (bottom panels) for $\chi^2 < 10$ and $\theta_{23} \leq 45^\circ$. Consistency with gauge unification is considered.

$$\begin{aligned}
 y_d : y_s : y_b &\sim \theta_C^8 : \theta_C^6 : \theta_C^3, \\
 \theta_{13}^q : \theta_{23}^q : \theta_{12}^q &\sim \theta_C^3 : \theta_C^2 : \theta_C^1,
 \end{aligned}
 \tag{3.20}$$

where θ_C is the Cabibbo angle. Taking these relations into account, we derive

$$\frac{\tilde{y}_\tau}{\tilde{y}_b} \approx \frac{r_2 + 3}{r_2 - 1} p - \frac{4r_1}{r_2 - 1} \frac{\tilde{y}_t}{\tilde{y}_b},
 \tag{3.21}$$

and from Eq. (3.7), where $\tilde{y}_f = \eta_f y_f$ where $\eta_f = \pm 1$ and

$$p = 1 - \frac{\tilde{y}_\mu}{\tilde{y}_\tau} + \frac{r_2 + 3}{r_2 - 1} \frac{\tilde{y}_s}{\tilde{y}_\tau},
 \tag{3.22}$$

which parametrises small deviations from 1 due to the suppressions of y_μ/y_τ and y_s/y_τ . We keep this deviation due to the fact that $y_\tau/y_b \approx 1$. We rewrite it in the form

$$r_2 \approx \frac{-4\tilde{y}_t}{\tilde{y}_\tau - \tilde{y}_b p} r_1 + \frac{\tilde{y}_\tau + 3\tilde{y}_b p}{\tilde{y}_\tau - \tilde{y}_b p},
 \tag{3.23}$$

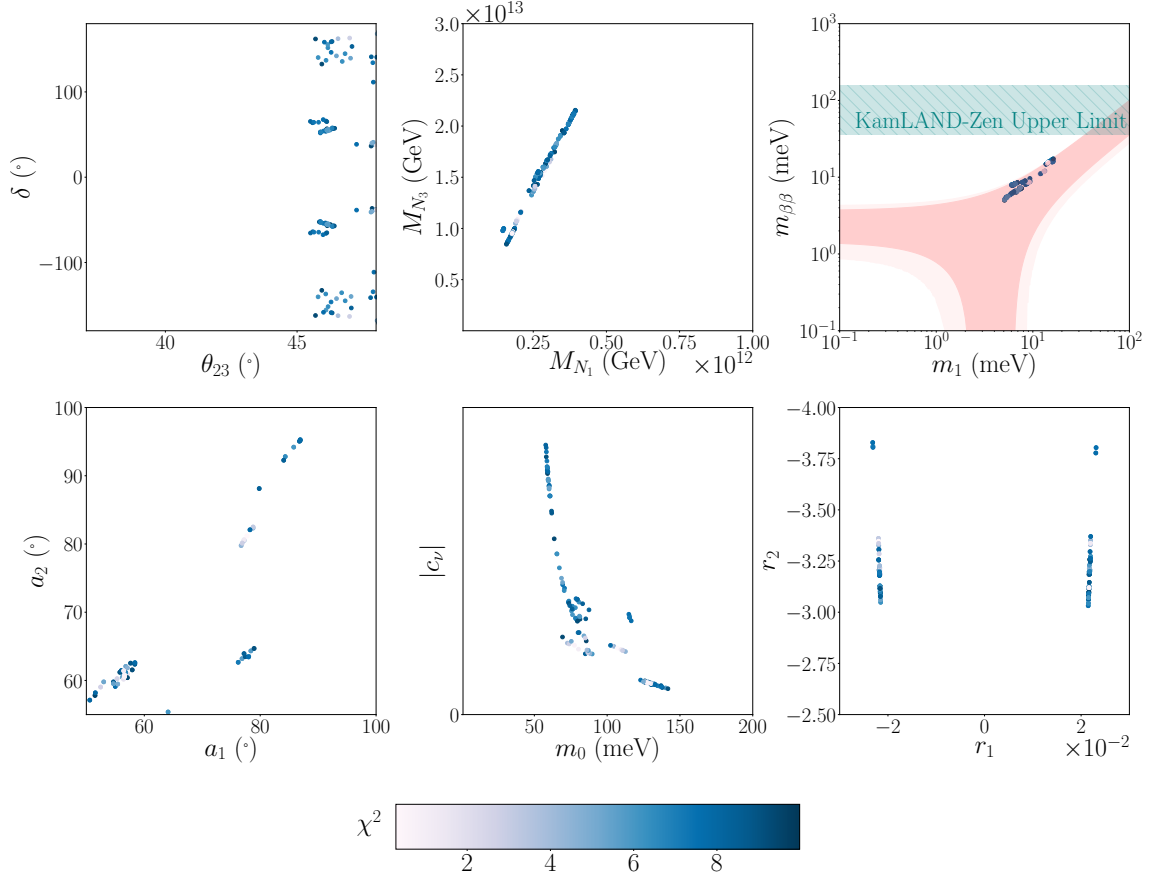


Figure 5: The predicted observables (top left two panels), the effective neutrino mass prediction (top right panel) and two-dimensional correlations between theory inputs (bottom panels) for $\chi^2 < 10$ and $\theta_{23} \geq 45^\circ$. Consistency with gauge unification is considered.

which provides an almost linear correlation between r_1 and r_2 , which is clearly shown in Fig. 5 for both $|\tilde{y}_\tau - \tilde{y}_b| = y_\tau - y_b$ and $y_\tau + y_b$. To satisfy the experimental constraint that $y_\tau/y_b \gtrsim 1$, most of the points with low χ^2 values satisfy the following hierarchical relation:

$$r_1 \ll 1 \ll r_2, \quad (3.24)$$

namely that $r_2 + 3/r_2 - 1 \approx 1$ and $|4r_1/r_2 - 1| \ll 1$. Using Eqs. (3.20) and (3.24), one can further derive approximate expressions for y_μ and y_e :

$$\begin{aligned} \tilde{y}_\mu &\approx \tilde{y}_s + \tilde{y}_b \sin^2 \theta_{23}^q (1 - c_e^2) \sin^2 a_2, \\ \tilde{y}_e &\approx [\tilde{y}_d + \tilde{y}_s \sin^2 \theta_{12}^q + \tilde{y}_b \sin^2 \theta_{13}^q (1 - c_e^2) \sin^2 a'_1] \\ &\quad - \frac{\tilde{y}_b^2}{\tilde{y}_\mu} \sin^2 \theta_{13}^q \sin^2 \theta_{23}^q [(\cos a'_1 \cos a_2 + c_e^2 \sin a'_1 \sin a_2)^2 + c_e^2 \sin^2(a'_1 - a_2)], \end{aligned} \quad (3.25)$$

where $a'_1 = a_1 - \delta^q$. However, the relation shown in Eq. (3.24) is not always satisfied as a few points with $r_2 \sim 0.13$ are also allowed by $\chi^2 < 10$ in our scan and this leads to $(r_2 + 3)/(r_2 - 1) \approx -3.6$.

Inputs	a_1	a_2	c_ν	m_0	$(\eta_u, \eta_c, \eta_t; \eta_d, \eta_s, \eta_b)$
	63.57°	84.17°	-1.945	82.82 meV	$(+, +, -; +, -, +)$
Outputs	θ_{13}	θ_{12}	θ_{23}	δ	m_1
	8.53°	32.7°	41.9°	-125°	3.36 meV
$(\chi^2 = 0.33)$	$m_{\beta\beta}$		M_{N_1}	M_{N_2}	M_{N_3}
	5.83 meV		$4.23 \cdot 10^{11}$ GeV	$5.32 \cdot 10^{11}$ GeV	$1.66 \cdot 10^{13}$ GeV

Table 6: Inputs and predictions of neutrino masses and mixing parameters of BP1 fully satisfy all experimental data. Charged fermion masses and CKM mixing are all fixed at experimental best-fit values. Neutrino masses with normal ordering are predicted.

The bottom-right panels of Figs. 4 and 5 show the prediction of the lightest neutrino mass, m_1 , and the effective mass parameter defined as:

$$m_{\beta\beta} = \left| \sum_{i=1}^3 m_i (U_{\text{PMNS}})_{ei}^2 \right|, \quad (3.26)$$

which neutrinoless double- β decay experiments can determine if neutrinos are Majorana as predicted by our model. m_1 is predicted to be less than 2 meV and $m_{\beta\beta} \sim (2, 20)$ meV. The above numerical analysis applies to only the normal ordering of light neutrino masses. We completed a preliminary scan for the inverted ordering and found that very few points had $\chi^2 < 100$ and did not proceed with a more dense scan. Although we have not proved that the GUT model disagrees with the inverted mass ordering, our model shows a preference for normal mass ordering given our scan.

3.3 The benchmark study

In this subsection, we study BP1 focusing on the flavour sector of quarks and leptons. Inputs and predictions of fermion Yukawas and mixing parameters are shown in Table 6 from which we obtain

$$\begin{aligned}
 h &= 10^{-2} \begin{pmatrix} -0.1934 & 0.1343 & -0.0845 \\ 0.1343 & 0.3924 & -0.0995 \\ -0.0845 & -0.0995 & -33.7016 \end{pmatrix}, \\
 f &= 10^{-2} \cdot \begin{pmatrix} -0.1934 & 0.1343 & -0.0845 \\ 0.1343 & 0.3924 & -0.0995 \\ -0.0845 & -0.0995 & -33.7016 \end{pmatrix}, \\
 h' &= 10^{-2} \cdot \begin{pmatrix} 0. & -0.0693 & 0.0025 \\ 0.0693 & 0. & -1.4430 \\ -0.0025 & 1.4430 & 0. \end{pmatrix}.
 \end{aligned}$$

From this, the Yukawa and neutrino mass matrices are obtained:

$$Y_u = \begin{pmatrix} 2.54 \cdot 10^{-6} & 0 & 0 \\ 0 & -0.00137 & 0 \\ 0 & 0 & -0.428 \end{pmatrix}, \quad (3.27)$$

$$Y_d = 10^{-2} \cdot \begin{pmatrix} 0.0056 & -0.0039 + 0.0014i & 0.0024 - 0.0i \\ -0.0039 - 0.0014i & -0.0100 & 0.0029 + 0.0281i \\ 0.0024 + 0.0i & 0.0029 - 0.0281i & 0.5686 \end{pmatrix}, \quad (3.28)$$

$$Y_e = 10^{-2} \cdot \begin{pmatrix} -0.0018 & 0.0012 - 0.0111i & -0.0008 + 0.004i \\ 0.0012 + 0.0111i & -0.0003 & -0.0009 - 0.2304i \\ -0.0008 - 0.0004i & -0.0009 + 0.2304i & 0.9155 \end{pmatrix}, \quad (3.29)$$

$$Y_\nu = 10^{-2} \cdot \begin{pmatrix} -0.7743 & 0.5374 + 0.1348i & -0.3379 - 0.0049i \\ 0.5374 - 0.1348i & 1.1586 & -0.3979 + 2.8068i \\ -0.3379 + 0.0049i & -0.3979 - 2.8068i & -6.4066 \end{pmatrix}, \quad (3.30)$$

$$M_\nu = 10^{-2} \cdot \begin{pmatrix} -0.5269 + 0.0i & 0.3628 + 0.0090i & -0.0434 - 0.0446i \\ 0.3628 + 0.0090i & 0.7407 - 0.0058i & -0.3755 - 2.417i \\ -0.0434 - 0.0446i & -0.3755 - 2.4168i & -2.9181 + 2.0125i \end{pmatrix} \text{ eV}. \quad (3.31)$$

Diagonalisation of Y_e and M_ν gives rise to the lepton masses and mixing, and the above benchmark provides $\chi^2 = 0.33$. We show predictions of charged lepton Yukawa couplings, mixing angles and the Dirac CP-violating phase, as well as the lightest neutrino mass m_1 and $m_{\beta\beta}$ in Table 6. Applying the type-I seesaw formula, the right-handed neutrino mass matrix is

$$M_{\nu_R} = 10^{13} \cdot \begin{pmatrix} -0.0354 & 0.0246 & -0.0154 \\ 0.0246 & 0.0467 & -0.0182 \\ -0.0154 & -0.0182 & 1.6650 \end{pmatrix} \text{ GeV}. \quad (3.32)$$

Moreover, the three associated eigenvalues are given in Table 6. Finally, we note that the heaviest right-handed neutrino mass is given by 1.6×10^{13} GeV. This is lower than the lowest intermediate scale M_1 and thus consistent with proton decay measurement.

4 Leptogenesis

As $SO(10)$ GUTs predict very massive right-handed neutrinos, leptogenesis is a natural consequence of such a framework. $SO(10)$ leptogenesis was initially studied in [42, 43]. Later, the importance of flavour effects was emphasised [44] and in [45] the same authors investigated the correlations between the viable $SO(10)$ leptogenesis parameter space and low-scale observables. Leptogenesis within a specific $SO(10)$ model, which fit low energy SM fermionic data [46], was investigated in [47]. Fitting leptogenesis together with all the fermion mass observables by solving density matrix equations was carried out in [48]. In this

section, we calculate the baryon asymmetry produced via thermal leptogenesis for the points of the parameter space scan, which are consistent with the quark and lepton experimental data with $\chi^2 < 10$ and later emphasise the connection between $SO(10)$ leptogenesis and observables such as proton decay and GWs.

To calculate the associated baryon-to-photon ratio, we solve the Boltzmann equations which determine the time evolution of the lepton asymmetry that manifests from the CP-violating and out-of-equilibrium decays of the right-handed neutrinos and associated washout processes. In the simplest formulation, these kinetic equations are in the one-flavoured regime, in which only a single flavour of charged lepton is accounted for. This regime is only realised at sufficiently high temperatures ($T \gg 10^{12}$ GeV) when the rates of processes mediated by the charged lepton Yukawa couplings are out of thermal equilibrium. Therefore, a single charged lepton flavour state is a coherent superposition of the three flavour eigenstates. However, if leptogenesis occurs at lower temperatures ($10^9 \ll T \ll 10^{12}$ GeV), scattering induced by the tau Yukawa couplings can cause the single charged lepton flavour to decohere, and the dynamics of leptogenesis must be described in terms of two flavour eigenstates. In such a regime, a density matrix formalism [49–53] allows for a more general description than the one-flavoured semi-classical Boltzmann equations. We begin by rotating the Yukawa coupling of the leptonic and Higgs doublet to the right-handed neutrinos mass basis. For example, the benchmark case in Eq. (3.30) is rotated to

$$\tilde{Y}_\nu = 10^{-2} \cdot \begin{pmatrix} 0.0547 + 0.9061i & 0.2923 - 0.2626i & 0.1159 - 0.1146i \\ -0.0024 + 0.04351i & -1.8277 + 0.1813i & -0.4079 + 1.2977i \\ -0.7770 - 0.2221i & 0.5467 + 2.3425i & -6.8722 - 0.0676i \end{pmatrix}. \quad (4.1)$$

The CP-asymmetry matrix, describing the decay asymmetry generated by N_i is denoted by $\epsilon_{\alpha\beta}^{(i)}$, and may be written as [54]:

$$\begin{aligned} \epsilon_{\alpha\beta}^{(i)} = & \frac{3}{32\pi \left(\tilde{Y}_\nu^\dagger \tilde{Y}_\nu\right)_{ii}} \sum_{j \neq i} \left\{ i \left[\tilde{Y}_{\nu\alpha i} \tilde{Y}_{\nu\beta j}^* \left(\tilde{Y}_\nu^\dagger \tilde{Y}_\nu\right)_{ji} - \tilde{Y}_{\nu\beta i}^* \tilde{Y}_{\nu\alpha j} \left(\tilde{Y}_\nu^\dagger \tilde{Y}_\nu\right)_{ij} \right] \frac{\xi(x_j/x_i)}{\sqrt{x_j/x_i}} \right. \\ & \left. + i \frac{2}{3(x_j/x_i - 1)} \left[\tilde{Y}_{\nu\alpha i} \tilde{Y}_{\nu\beta j}^* \left(\tilde{Y}_\nu^\dagger \tilde{Y}_\nu\right)_{ij} - \tilde{Y}_{\nu\beta i}^* \tilde{Y}_{\nu\alpha j} \left(\tilde{Y}_\nu^\dagger \tilde{Y}_\nu\right)_{ji} \right] \right\}, \end{aligned} \quad (4.2)$$

where $x_i \equiv M_{N_i}^2/M_{N_1}^2$ and Greek and Roman indices denote charged lepton flavour and right-handed neutrino generation indices, respectively, and

$$\xi(x) = \frac{2}{3}x \left[(1+x) \ln \left(\frac{1+x}{x} \right) - \frac{2-x}{1-x} \right]. \quad (4.3)$$

N^{B-L} is a density matrix parametrising the lepton asymmetries in flavour space, and $\mathcal{P}^{(i)0}$ denotes the projection matrices which describe how a given flavour of lepton is washed out:

$$N^{B-L} = \begin{pmatrix} N_{\tau\tau} & N_{\tau\mu} & N_{\tau e} \\ N_{\mu\tau} & N_{\mu\mu} & N_{\mu e} \\ N_{e\tau} & N_{e\mu} & N_{ee} \end{pmatrix}, \quad \mathcal{P}^{(i)0} = \frac{1}{\left(\tilde{Y}_\nu^\dagger \tilde{Y}_\nu\right)_{ii}} \begin{pmatrix} \left|\tilde{Y}_{\nu\tau i}\right|^2 & \tilde{Y}_{\nu\tau i} \tilde{Y}_{\nu\mu i}^* & \tilde{Y}_{\nu\tau i} \tilde{Y}_{\nu e i}^* \\ \tilde{Y}_{\nu\tau i}^* \tilde{Y}_{\nu\mu i} & \left|\tilde{Y}_{\nu\mu i}\right|^2 & \tilde{Y}_{\nu\tau i}^* \tilde{Y}_{\nu e i} \\ \tilde{Y}_{\nu e i} \tilde{Y}_{\nu\tau i}^* & \tilde{Y}_{\nu\mu i} \tilde{Y}_{\nu\tau i}^* & \left|\tilde{Y}_{\nu e i}\right|^2 \end{pmatrix}. \quad (4.4)$$

Finally, the density matrix equations which track the time evolution of the lepton asymmetry generated by the decays and washout of the three right-handed neutrinos are given by:

$$\begin{aligned} \frac{dN_{\alpha\beta}^{B-L}}{dz} = & \sum_{i=1}^3 \varepsilon_{\alpha\beta}^{(i)} D_i \left(N_{N_i} - N_{N_i}^{\text{eq}} \right) - \frac{1}{2} W_i \left\{ \mathcal{P}^{(i)0}, N^{B-L} \right\}_{\alpha\beta} \\ & - \frac{\text{Im}(\Lambda_\tau)}{Hz} \left[\begin{pmatrix} 1 & 0 & 0 \\ 0 & 0 & 0 \\ 0 & 0 & 0 \end{pmatrix}, \begin{pmatrix} 1 & 0 & 0 \\ 0 & 0 & 0 \\ 0 & 0 & 0 \end{pmatrix}, N^{B-L} \right]_{\alpha\beta} \\ & - \frac{\text{Im}(\Lambda_\mu)}{Hz} \left[\begin{pmatrix} 0 & 0 & 0 \\ 0 & 1 & 0 \\ 0 & 0 & 0 \end{pmatrix}, \begin{pmatrix} 0 & 0 & 0 \\ 0 & 1 & 0 \\ 0 & 0 & 0 \end{pmatrix}, N^{B-L} \right]_{\alpha\beta}, \end{aligned}$$

where $z = M_{N_1}/T$ is the evolution parameter, H is the Hubble expansion rate, and the decay and washout terms are given by

$$D_i(z) = K_i x_i z \frac{\mathcal{K}_1(z_i)}{\mathcal{K}_2(z_i)}, \quad W_i(z) = \frac{1}{4} K_i \sqrt{x_i} \mathcal{K}_1(z_i) z_i^3, \quad (4.5)$$

where $z_i \equiv \sqrt{x_i} z$, \mathcal{K}_1 and \mathcal{K}_2 are modified Bessel functions of the second kind with the decay asymmetry K_i given by

$$K_i \equiv \frac{\tilde{\Gamma}_i}{H(T = M_{N_i})}, \quad \tilde{\Gamma}_i = \frac{M_{N_i} \left(\tilde{Y}_\nu^\dagger \tilde{Y}_\nu \right)_{ii}}{8\pi}, \quad (4.6)$$

respectively. The thermal widths of the charged leptons, Λ_τ , Λ_μ , are given by the imaginary part of the self-energy correction to the charged lepton propagators in the plasma, and this mediates flavour correlations (for further details of these equations and their application we refer the reader to Ref. [56]).

For each point in our parameter scan, we have solved Eq. (4.5) which provides the baryon-to-photon ratio using the publicly available tool ULYSSES [57] and the associated ‘‘3DME’’ code which accounts for the decays and washout of all three right-handed neutrinos. We show our results in Fig. 6 where all the points have $\chi^2 < 10$ and satisfy the proton decay bounds. We observe that for both octants, many low χ^2 points achieve thermal leptogenesis successfully, and their baryon-to-photon ratio is $\eta_B \approx 10^{-10}$. Interestingly, the predicted baryon-to-photon ratio shows little dependence on δ but has a very constrained prediction for the effective Majorana mass, $4 \lesssim m_{\beta\beta} \text{ (meV)} \lesssim 10$. This indicates that the predicted Majorana phases are highly constrained within our model.

For all the points with $\chi^2 < 10$, we found leptogenesis is always in the strong washout regime $K_1 \gg 1$ (for the benchmark point $K_1 \approx 130$) since the Yukawa couplings (Eq. (3.30)) are not very small. As we are in the strong washout regime, neglecting finite density effects is a good approximation [58]. For the above benchmark point, the lightest two masses of right-handed neutrinos are $M_{N_1} = 4.23 \cdot 10^{11}$ GeV and $M_{N_2} = 5.32 \cdot 10^{11}$ GeV and the baryon-to-photon ratio is $\sim 6.11 \times 10^{-10}$. Next generation $0\nu\beta\beta$ experiments such as

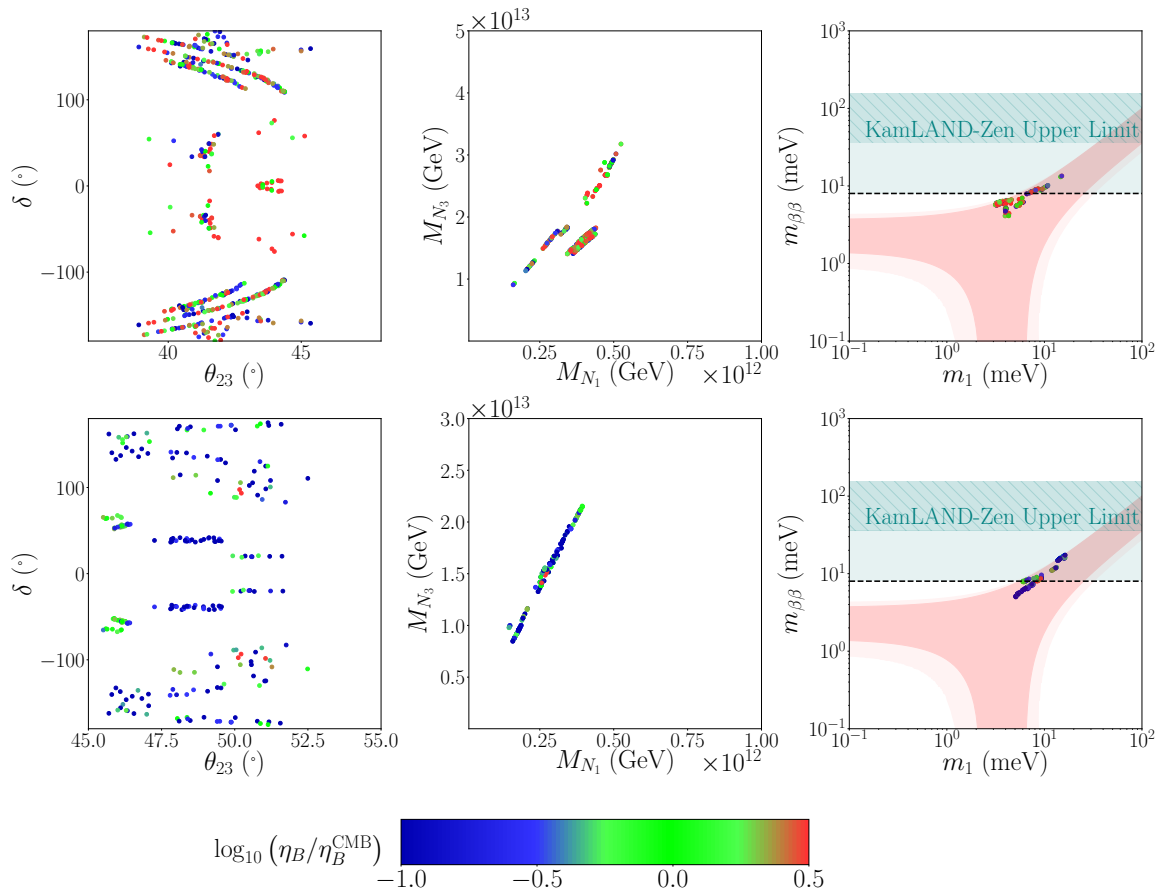


Figure 6: The top (bottom) left and centre panels are the two-dimensional correlations between predicted observables for $\chi^2 < 10$ and $\theta_{23} \leq 45^\circ$ ($\theta_{23} \geq 45^\circ$). The top (bottom) rightmost panel shows the predictions for the effective neutrino mass for $\theta_{23} \leq 45^\circ$ ($\theta_{23} \geq 45^\circ$). The colour of the points denotes the ratio of the predicted baryon-to-photon ratio to the experimentally observed best-fit value as measured using CMB data $\eta_B^{\text{CMB}} = 6.15 \times 10^{-10}$ [55]. Consistency with gauge unification is considered. In the leftmost plots, the dashed line labels the sensitivity of the next generation experiments on $0\nu\beta\beta$ decay.

Legend-1000 [59], nEXO [60], NEXT-HD [61], DARWIN[62], SNO+II [63] and CUPID-Mo [64] will allow to test further test the results of our scan. The most sensitive experiments will probe $m_{\beta\beta}$ down to 8 – 10meV which, as we can see from Fig. 6, covers a significant fraction of the points of our scan.

5 Testability of $SO(10)$ GUT and leptogenesis using gravitational waves

The creation of topological defects in GUT symmetry breaking is ubiquitous [7] and in our breaking chain produces unwanted defects in the breaking of $SO(10) \rightarrow G_2$ (monopoles and domain walls), but in the final breaking, $G_1 \rightarrow G_{\text{SM}}$, cosmic strings are formed. We assume

that inflation occurs after the unwanted defects are formed but before string formation.⁴ Under this assumption, the string network can intersect to form loops which oscillate and emit energy gravitational radiation that can constitute a stochastic gravitational wave background. Importantly, this background can, in principle, be observed by currently running and future GW experiments.

We assume the Nambu-Goto string approximation, where the string is infinitely thin with no couplings to particles [68], and the amplitude of the relic GW density parameter is:

$$\Omega_{\text{GW}}(f) = \frac{1}{\rho_c} \frac{d\rho_{\text{GW}}}{d \log f}, \quad (5.1)$$

where ρ_c is the critical energy density of the Universe and ρ_{GW} depends on a single parameter, $G\mu$ where $G = M_{\text{pl}}^{-2}$ is Newton's constant and μ is the string tension. For strings generated from the gauge symmetry $G_1 = SU(3)_c \times SU(2)_L \times SU(2)_R \times U(1)_X$.

$G\mu$ is approximately given by [69]:

$$G\mu \simeq \frac{1}{2(\alpha_{2R}(M_1) + \alpha_{1X}(M_1))} \frac{M_1^2}{M_{\text{pl}}^2}, \quad (5.2)$$

and hence we can relate the string tension parameter to the lowest intermediate scale of GUT symmetry breaking. The spectrum of $\Omega_{\text{GW}}(f)$ is calculated numerically by solving the formulation in [70] and [11, 12]. A well-known feature is at the high-frequency band, $\Omega_{\text{GW}}(f)$ has a $G\mu$ -dependent plateau [71]. In our calculations, we derive a semi-analytical correlation

$$(\Omega_{\text{GW}} h^2)_{\text{plateau}} \approx 6.5 \cdot 10^{-6} \times (G\mu)^{1/2} \sim 2.06 \cdot 10^{-5} \times \frac{M_1}{M_{\text{pl}}}, \quad (5.3)$$

where numerical values $\alpha_{2R} \sim \alpha_{1X} \sim 1/40$ around the scale M_1 have been accounted for. A GW background with $(\Omega_{\text{GW}} h^2)_{\text{plateau}} \sim 10^{-10}$ is naturally predicted from cosmic strings from the breaking scale $M_1 \sim 10^{13}$ GeV.⁵ There is an important relationship between the string loop length (l) at the time of formation (t_i), which is usually taken as a linear relation: $l = \alpha t_i$. While α has a distribution of values, it peaks at around 0.1 for both matter and radiation-dominated eras [72].

$G\mu$, or equivalently M_1 , should be restricted to a specific range as its value must be consistent with proton decay measurement and fermion masses and mixing data. For the breaking chain we consider, the upper bound is $M_1^{\text{upper}} \simeq 4.4 \times 10^{13}$ GeV from the proton decay. We account for a perturbativity ansatz for Majorana Yukawa coupling, i.e.,

⁴Studies on inflated cosmic strings are discussed in Refs. [11, 65–67].

⁵We note that the non-perturbative production of monopoles can modify the gravitational wave signature from GUT models [9], but this occurs if the monopole and cosmic string generation scales are not well separated. In our GUT model, monopole and string formation are well separated, and we assume a rapid period of inflation between these scales to remove the monopoles.

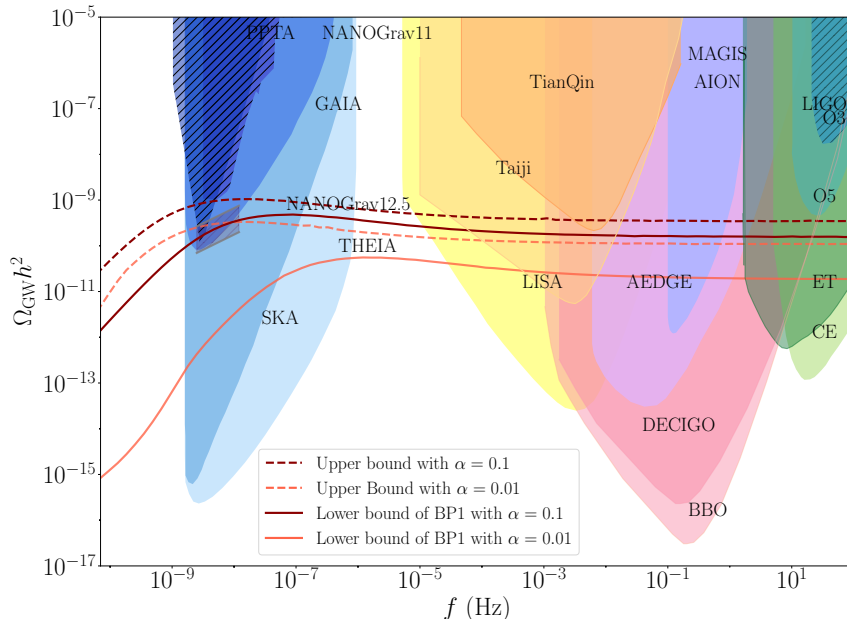


Figure 7: Gravitational wave spectrum predicted from the model. Breaking of the intermediate symmetry $G_1 \equiv SU(3)_c \times SU(2)_L \times SU(2)_R \times U(1)_X$ generates cosmic strings with tension μ . The lower bound to the GW spectrum for the benchmark point we considered earlier (red lines) is $G\mu = 2.68 \times 10^{-11}$ corresponding to $M_1 \simeq 2 \times 10^{13}$ GeV. The GW spectrums of these two bounds are shown in dashed and solid curves, respectively.

$M_{N_i} < M_1$ for all right-handed neutrinos.⁶ In this ansatz, the lower bound of M_1 is obtained as $M_1 > M_1^{\text{lower}} \equiv M_{N_3}$. This value varies with different scatter points shown in Figs. 4 and 5. For the benchmark point BP1, we take $M_1^{\text{lower}}(\text{BP1}) \simeq 2 \times 10^{13}$ GeV and obtain $G\mu \simeq 2.68 \times 10^{-11}$. The associated $\Omega_{\text{GW}}(f)h^2$ is shown in Fig. 7 with dashed and solid curves, where the coloured (hatched) regions indicate future (current) experimental sensitivities.

The prediction of $\Omega_{\text{GW}}h^2$ depends on the loop size parameter α . While simulations [71, 72] show this parameter peaks around $\alpha \approx 1$. Deviation could be considered as there could be some uncertainties in the peak value and distribution around it. A smaller value of α reduces the GW intensity as $\Omega_{\text{GW}} \approx \sqrt{\alpha}$. In the plot, we consider the case with the value $\alpha = 0.01$ (light red) as a comparison to the main result derived at $\alpha = 0.1$ (red).

⁶The Majorana Yukawa couplings for right-handed neutrinos connect the seesaw scale with the $U(1)_{B-L}$ scale. These couplings, in general, have an upper bound $\lesssim \mathcal{O}(1)$ to satisfy the perturbativity requirement. To obtain the bound explicitly, one has to consider the RG behaviour of Yukawa couplings and include the influence of Yukawa couplings on gauge unification. This procedure is complicated, and we relegate this for future work. In this work as an alternative, we consider a simplified perturbative ansatz by requiring the heaviest right-handed neutrino mass lighter than the $U(1)_{B-L}$ scale, i.e., $M_{N_3} < M_1$.

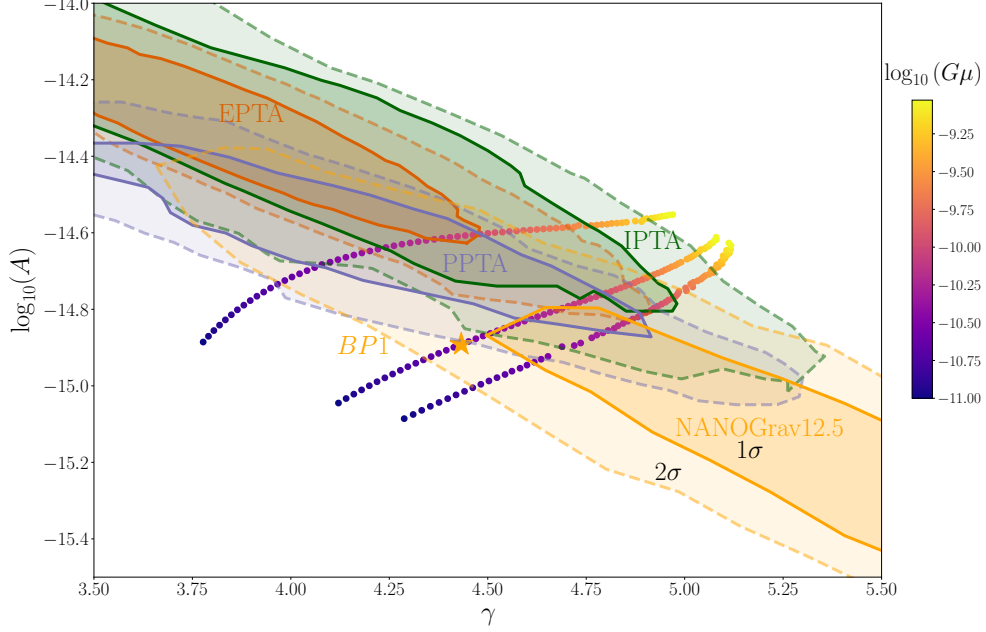


Figure 8: Comparison between SGWB signals produced by cosmic strings with $G\mu$ from 10^{-11} to 10^{-9} the possible 1σ and 2σ regions hinted by EPTA, PPTA, IPTA and NANOGrav. The SGWB signal has been fitted for three frequencies: 2.4 nHz, 5.4 nHz and 12 nHz. The simulation shows that the signal is compatible with all experiments at 2σ . The orange star indicates the prediction of (γ, A) in BP1.

A series of GW observatories, including space-based laser interferometers (LISA [73], Taiji [74], TianQin [75], BBO [76], DECIGO [77]), atomic interferometers (MAGIS [78], AEDGE [79], AION [80]), and ground-based interferometers (Einstein Telescope [81] (ET), Cosmic Explorer [82] (CE)) will cover GW frequency band from mHz to kHz and probe $G\mu$ values in a wide range $\sim 10^{-19} - 10^{-11}$, as seen in Fig. 7. A combined analysis of these experiments can potentially exclude cosmic strings-originated GW signals to high sensitivity.

Data from pulsar timing arrays (PTA) such as EPTA [83] and NANOGrav (11-year data set) [19] have already probed the nHz regime and provided upper limits through the non-observation of GWs. Future PTA such as SKA [84] will cover even more parameter space, and large-scale surveys of stars such as Gaia [85] and the proposed upgrade, THEIA [86], can be powerful and complementary probes of gravitational waves in the same frequency regime.

The PTA experiment NANOGrav released its 12.5-year data set [14] which announced the detection of a common-spectrum process that has a characteristic strain of the form

$$h_c(f) = A \left(\frac{f}{f_{\text{yr}}} \right)^\alpha, \quad (5.4)$$

where $f_{\text{yr}} = 1/\text{year}$, and A is an amplitude parameter referring to the correlation between

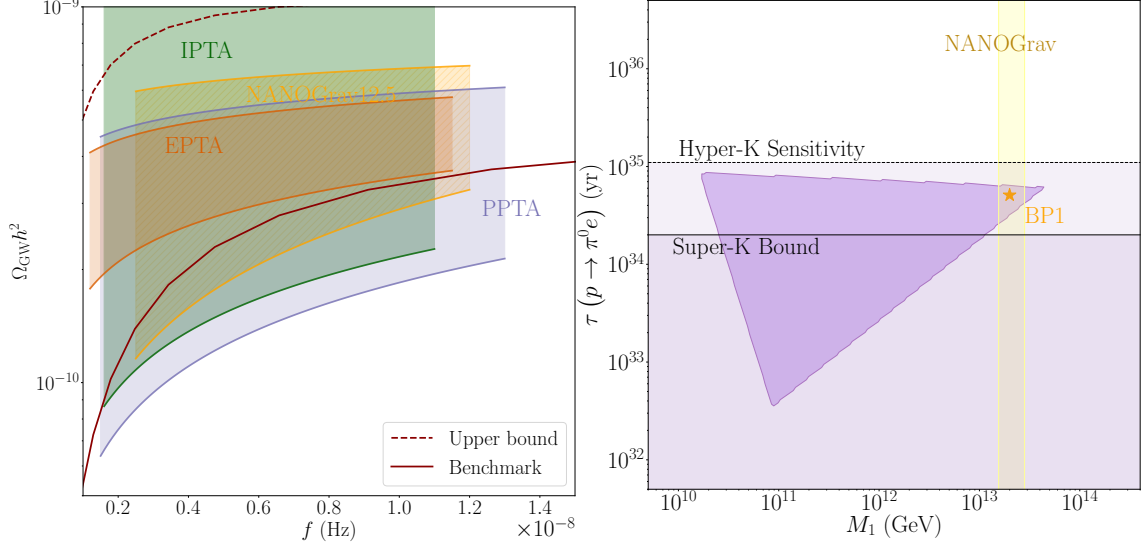


Figure 9: Left: Blown-up image of the nHz region of the gravitational waves spectrum of the benchmark point and the upper bound. This is compared with the region of EPTA, IPTA, PPTA and NANOGrav consistent with the observation of an SGWB. Right: Proton decay lifetime compared with the region of M_1 consistent with NANOGrav12.5, we can see that there is a region of the parameter space which can be tested by Hyper-K, which is consistent with NANOGrav. The orange star indicates BP1.

pulsars. If this signal is confirmed as a cosmic GW background, the characteristic strain can be transformed into the GW energy density:

$$(\Omega_{\text{GW}}(f)h^2)_{\text{PTA}} \approx 2.02 \cdot 10^{-10} \left(\frac{A}{10^{-15}} \right)^2 \times \left(\frac{f}{f_{\text{yr}}} \right)^{5-\gamma}, \quad (5.5)$$

where $\gamma = 3 - 2\alpha$. Motivated by searches for supermassive black hole mergers, the cross-power spectral density can be fixed at $\gamma = 13/3$ and A as measured by NANOGrav is

$$A = 1.92_{-0.55}^{+0.75} \times 10^{-15}, \quad \gamma = \frac{13}{3} \text{ fixed (NANOGrav)} \quad (5.6)$$

at 95% CL. This range of A has recently been confirmed by other pulsar-timing arrays including PPTA [15, 87], EPTA [16] and IPTA [17] without fixing the value of α or γ . At 95% CL, A and γ in these experiments are fitted to be

$$\begin{aligned} A &= 2.82_{-1.16}^{+0.73} \times 10^{-15}, & \gamma &= 4.11_{+0.52}^{-0.41} & (\text{PPTA}), \\ A &= 5.13_{-2.73}^{+4.20} \times 10^{-15}, & \gamma &= 3.78_{+0.69}^{-0.59} & (\text{EPTA}), \\ A &= 3.8_{-2.5}^{+6.3} \times 10^{-15}, & \gamma &= 4.0_{+0.9}^{-0.9} & (\text{IPTA}), \end{aligned} \quad (5.7)$$

respectively.

These data hint at a GW energy density $\Omega_{\text{GW}} h^2 \sim 10^{-10}$ in the nHz band. The hinted ranges of A and γ are highly correlated in all these experiments. We include 1σ and 2σ

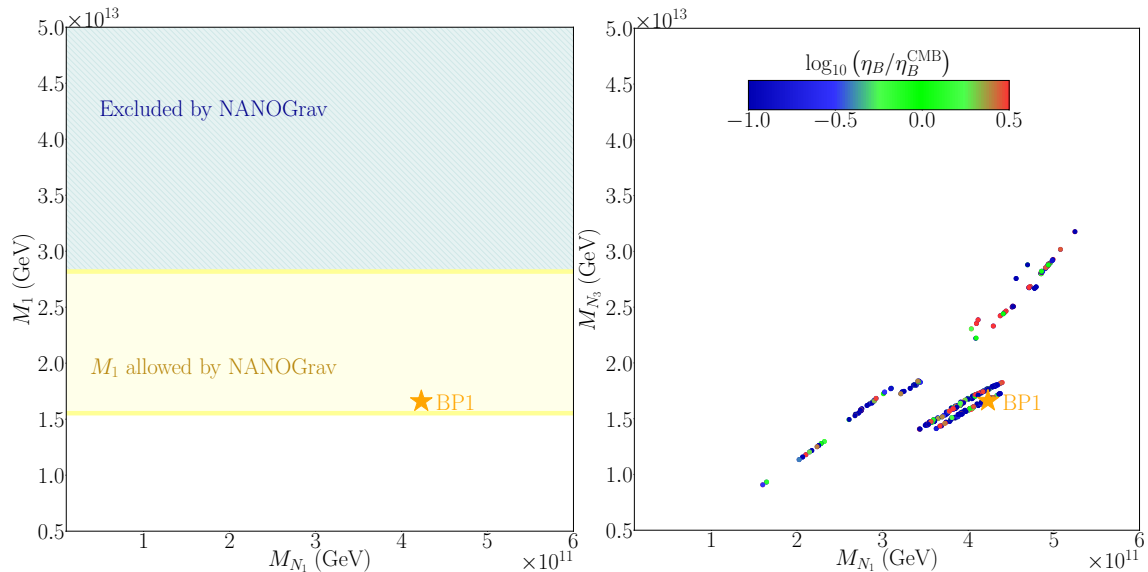


Figure 10: Comparison between the results of our scan and NANOGrav12.5 bound. The yellow shaded region includes all the values of M_1 consistent with NANOGrav. Applying the perturbativity ansatz, i.e., $M_1 > M_{N_3}$, we can see how most of the points in our scan are consistent with NANOGrav. The first octant of lepton mixing angle θ_{23} is considered.

regions of (γ, A) restricted by these measurements in Fig. 8. In the same figure, we also present three dotted curves which show how the $G\mu$, associated with cosmic strings, overlays on the A - γ regions of various experiments. Following the treatment used in [88] the curves are obtained as follows: for a given value of $G\mu$, the spectrum of $\Omega_{\text{GW}}(f)h^2$ is obtained from our numerical calculation, A and γ are reversely calculated via Eq. (5.5) by fixing the frequency $f = f_*$. In particular, γ is solved via $\gamma = 5 - \frac{\partial \log \Omega_{\text{GW}}(f)}{\partial \log f} \Big|_{f_*}$. We set $f_* = 2.4, 5.6$ and 12 nHz, respectively, vary $G\mu$ from 10^{-11} to 10^{-9} , and obtain three curves respectively, shown in Fig. 8 where the second frequency is the one considered in [88] and the first and third refer to the first and the fifth lowest frequencies measured in NANOGrav12.5. The overlap between these curves and the PTA hinted regions indicate the consistency between cosmic-string-sourced SGWB signal and the experimental searches. For $f_* = 5.6$ nHz, we found that the signal is compatible with NANOGrav12.5, PPTA and IPTA in 1σ and EPTA in 2σ ranges. A and γ in 2σ ranges are restricted in

$$\begin{aligned}
 A &= (1.75, 1.95) \times 10^{-15}, & \gamma &= (4.34, 4.90) & (\text{NANOGrav}), \\
 A &= (1.32, 1.85) \times 10^{-15}, & \gamma &= (4.44, 4.86) & (\text{PPTA}), \\
 A &= (1.56, 1.82) \times 10^{-15}, & \gamma &= (4.68, 4.85) & (\text{EPTA}), \\
 A &= (1.38, 2.24) \times 10^{-15}, & \gamma &= (4.50, 5.03) & (\text{IPTA}),
 \end{aligned} \tag{5.8}$$

respectively. Here, upper bounds of A and γ in NANOGrav and IPTA are not considered as they predict $\Omega_{\text{GW}}h^2 > 10^{-9}$ which are too large for our interests. We apply these ranges to Eq. (5.5), and in the left panel of Fig. 9 we show a zoom-in of the upper bound and BP1

GW signal intersecting the various PTA experimental sensitivities. We observe that our benchmark point can explain the possible signal observed. In the right panel of Fig. 9 we show our GUT model's predicted proton lifetime as a function of M_1 .

In the left panel of Fig. 10, we show the range of M_1 values predicted by our model, where the yellow shows the region consistent with the NANOGrav 12.5-year data set. As there is a degree of freedom which relates M_1 and M_{N_1} that we cannot constrain, there is a range of lightest right-handed neutrino masses that can accommodate this GW signal. In the right panel, we show how our leptogenesis prediction lies in the $M_{N_1} - M_{N_3}$ plane.

In Fig. 10, we present the plot of leptogenesis vs RHN neutrino masses M_{N_1} and M_{N_3} and include the M_1 upper bound required by NANOGrav for the first (left panel) and second (right panel) octant. The heaviest RHN neutrino mass M_{N_3} should not be larger than M_1 and thus not larger than the upper bound of M_1 . Importantly, the RHN masses which give viable leptogenesis are in the region of the PS testable by NANOGrav12.5.

Finally, we briefly discuss the GW signal predicted by the benchmark point. Given the lowest and the second lowest intermediate scales $M_1 = 2 \times 10^{13}$ GeV and $M_2 = 5 \times 10^{13}$ GeV and the consistency with gauge unification, $G\mu$ is predicted to be 1.1×10^{-10} which corresponds to $\Omega_{\text{GW}}(f)h^2 \sim 4.2 \times 10^{-10}$ at the peak around 6.3×10^{-7} Hz. This is a critical value to be tested in the PTA experiments. In the high frequency band, $\Omega_{\text{GW}}(f)h^2 \sim 1.6 \times 10^{-10}$ is predicted. The future space-based, atomic and underground-based GW observatories will give an excellent test of this value.

6 Discussion and conclusion

Grand Unified Theories offer an attractive ultraviolet completion of the Standard Model and can explain the masses and mixings of the known particles. In our former works, we proposed gravitational wave and proton decay measurements as complementary windows to identify possible breaking chains of GUTs [11] and provided a systematic analysis for all $SO(10)$ chains via the Pati-Salam-type breaking. In addition, we focused on the connection between the proton lifetime and stochastic GW background energy density [12].

In this paper, we perform a detailed analysis of one such $SO(10)$ GUT breaking chain involving a realistic and minimal $SO(10)$ GUT model which breaks to the Standard Model gauge group via three intermediate gauge symmetries. Four Higgs multiplets are required to induce the desired pattern of breaking. An additional two Higgs multiplets are introduced for our model to predict the SM fermion masses and mixing to a high statistical significance. From the constraint of gauge unification and proton decay, and including the relevant particles in our two-loop renormalisation group equations, we determine the scale of spontaneous symmetry breaking from our GUT model to the Standard Model. The final intermediate symmetry breaking induces a network of cosmic string, which results in the emission of GWs, assuming that inflation ends earlier than string formation. Our numerical procedure uses the quark masses and mixing as constraints on our GUT model parameter space (four-dimensional). We performed a grid scan of this space and found that

neutrino masses and mixing (five observables) can be accommodated to a high statistical significance. Once the viable regions of the model parameter space were found and the intermediate scales determined, we have a fixed prediction for leptogenesis, gravitational waves and proton decay.

Our scan result shows that the right-handed neutrino spectrum can be strongly restricted as the model has to fit all flavour data, including fermion masses, CKM mixing and PMNS mixing. The heaviest right-handed neutrino mass is predicted to be in a narrow region above 10^{13} GeV. Given the chosen breaking chain, this region is still consistent with the upper bound of the lowest intermediated scale restricted by proton decay and GW measurements. It is worth emphasising that recently released data from a series of Pulsar Timing Arrays measurements hints at this region. However, more data is required to confirm if these signals are from a stochastic GW background. In the future, both proton decay measurement experiment Hyper-K and GW observatories can exclude or confirm this region. Furthermore, the latter has the potential to provide powerful constraints to many GUT models.

Throughout, we present a benchmark point, BP1, which satisfies all experimental constraints, including proton decay, quark masses and mixing, lepton masses and mixing and can address the observed matter-antimatter asymmetry in the Universe. By fixing intermediate scales at 2×10^{13} and 5×10^{13} GeV, respectively, the GUT breaking scale is solved to be around 5.68×10^{15} GeV, and the proton lifetime is predicted to be around 5.1×10^{34} years, which survives the upper bound restricted by Super-K and will be tested in Hyper-K in the future. This benchmark predicts three right-handed neutrino masses $(M_{N_1}, M_{N_2}, M_{N_3}) = (4.23 \cdot 10^{11}, 5.32 \cdot 10^{11}, 1.66 \cdot 10^{13})$ GeV. These heavy neutrinos, together with their CP-violating Yukawa couplings with active neutrinos, can explain the baryon-antibaryon asymmetry of the Universe quantitatively via leptogenesis. The mass of the heaviest right-handed neutrino is lower than the lowest intermediate scale M_1 , thus consistent with the Super-K constraint on proton decay.

In summary, we are entering an exciting era where the culmination of data from proton decay, gravitational wave and neutrinoless double beta decay experiments will allow us to test Grand Unification and its connection with the matter-antimatter asymmetry at unprecedented levels. To illustrate this, we have analysed in full detail a specific example of a realistic and minimal SO(10) model broken to the SM via three intermediate scales, and shown that it will be tested very soon by such experiments. Given the upcoming synergy in experimental data it is of interest to extend our methodology to further GUT models.

Acknowledgement

This work was partially supported by the European Union’s Horizon 2020 Research and Innovation Programme under Marie Skłodowska-Curie grant agreement HIDDEN European ITN project (H2020-MSCA-ITN-2019//860881-HIDDEN), the European Research Council under ERC Grant NuMass (FP7-IDEAS-ERC ERC-CG 617143). S. F. K. acknowl-

edges the STFC Consolidated Grant ST/T000775/1. Y. L. Z. was supported by the National Natural Science Foundation of China under grants No. 12205064. B. F. acknowledges the Chinese Scholarship Council (CSC) Grant No. 201809210011 under agreements [2018]3101 and [2019]536. This work used the DiRAC@Durham facility managed by the Institute for Computational Cosmology on behalf of the STFC DiRAC HPC Facility (www.dirac.ac.uk). The equipment was funded by BEIS capital funding via STFC capital grants ST/P002293/1, ST/R002371/1 and ST/S002502/1, Durham University and STFC operations grant ST/R000832/1. DiRAC is part of the National e-Infrastructure. Y. L. Z. would like to thank J. Liu for useful discussion.

References

- [1] H. Georgi and S.L. Glashow, Unified weak and electromagnetic interactions without neutral currents, *Phys. Rev. Lett.* **28** (1972) 1494.
- [2] S.M. Barr, A New Symmetry Breaking Pattern for SO(10) and Proton Decay, *Phys. Lett.* **112B** (1982) 219.
- [3] J. Derendinger, J.E. Kim and D.V. Nanopoulos, Anti-SU(5), *Phys. Lett. B* **139** (1984) 170.
- [4] A. De Rujula, H. Georgi and S. Glashow, FLAVOR GONIOMETRY BY PROTON DECAY, *Phys. Rev. Lett.* **45** (1980) 413.
- [5] I. Antoniadis, J.R. Ellis, J. Hagelin and D.V. Nanopoulos, The Flipped SU(5) x U(1) String Model Revamped, *Phys. Lett. B* **231** (1989) 65.
- [6] J.C. Pati and A. Salam, Unified Lepton-Hadron Symmetry and a Gauge Theory of the Basic Interactions, *Phys. Rev. D* **8** (1973) 1240.
- [7] R. Jeannerot, J. Rocher and M. Sakellariadou, How generic is cosmic string formation in SUSY GUTs, *Phys. Rev.* **D68** (2003) 103514 [[hep-ph/0308134](https://arxiv.org/abs/hep-ph/0308134)].
- [8] M. Fukugita and T. Yanagida, Baryogenesis Without Grand Unification, *Phys. Lett.* **B174** (1986) 45.
- [9] W. Buchmuller, V. Domcke, H. Murayama and K. Schmitz, Probing the scale of grand unification with gravitational waves, *Phys. Lett. B* **809** (2020) 135764 [[1912.03695](https://arxiv.org/abs/1912.03695)].
- [10] J.A. Dror, T. Hiramatsu, K. Kohri, H. Murayama and G. White, Testing the Seesaw Mechanism and Leptogenesis with Gravitational Waves, *Phys. Rev. Lett.* **124** (2020) 041804 [[1908.03227](https://arxiv.org/abs/1908.03227)].
- [11] S.F. King, S. Pascoli, J. Turner and Y.-L. Zhou, Gravitational Waves and Proton Decay: Complementary Windows into Grand Unified Theories, *Phys. Rev. Lett.* **126** (2021) 021802 [[2005.13549](https://arxiv.org/abs/2005.13549)].
- [12] S.F. King, S. Pascoli, J. Turner and Y.-L. Zhou, Confronting SO(10) GUTs with proton decay and gravitational waves, *JHEP* **10** (2021) 225 [[2106.15634](https://arxiv.org/abs/2106.15634)].
- [13] SUPER-KAMIOKANDE collaboration, Search for proton decay via $p \rightarrow e^+\pi^0$ and $p \rightarrow \mu^+\pi^0$ with an enlarged fiducial volume in Super-Kamiokande I-IV, *Phys. Rev. D* **102** (2020) 112011 [[2010.16098](https://arxiv.org/abs/2010.16098)].

- [14] NANOGrav collaboration, The NANOGrav 12.5-year Data Set: Search For An Isotropic Stochastic Gravitational-Wave Background, [2009.04496](#).
- [15] B. Goncharov et al., On the Evidence for a Common-spectrum Process in the Search for the Nanohertz Gravitational-wave Background with the Parkes Pulsar Timing Array, [Astrophys. J. Lett. **917** \(2021\) L19 \[2107.12112\]](#).
- [16] S. Chen et al., Common-red-signal analysis with 24-yr high-precision timing of the European Pulsar Timing Array: inferences in the stochastic gravitational-wave background search, [Mon. Not. Roy. Astron. Soc. **508** \(2021\) 4970 \[2110.13184\]](#).
- [17] J. Antoniadis et al., The International Pulsar Timing Array second data release: Search for an isotropic gravitational wave background, [Mon. Not. Roy. Astron. Soc. **510** \(2022\) 4873 \[2201.03980\]](#).
- [18] R.N. Manchester et al., The Parkes Pulsar Timing Array Project, [Publ. Astron. Soc. Austral. **30** \(2013\) 17 \[1210.6130\]](#).
- [19] NANOGrav collaboration, The NANOGrav 11-year Data Set: Pulsar-timing Constraints On The Stochastic Gravitational-wave Background, [Astrophys. J. **859** \(2018\) 47 \[1801.02617\]](#).
- [20] HYPER-KAMIOKANDE collaboration, Hyper-Kamiokande Design Report, [1805.04163](#).
- [21] F. del Aguila and L.E. Ibanez, Higgs Bosons in SO(10) and Partial Unification, [Nucl. Phys. B **177** \(1981\) 60](#).
- [22] R.D. Peccei and H.R. Quinn, CP Conservation in the Presence of Instantons, [Phys. Rev. Lett. **38** \(1977\) 1440](#).
- [23] A.S. Joshipura and K.M. Patel, Fermion Masses in SO(10) Models, [Phys. Rev. D **83** \(2011\) 095002 \[1102.5148\]](#).
- [24] B. Bajc, A. Melfo, G. Senjanovic and F. Vissani, Yukawa sector in non-supersymmetric renormalizable SO(10), [Phys. Rev. D **73** \(2006\) 055001 \[hep-ph/0510139\]](#).
- [25] K.S. Babu and R.N. Mohapatra, Predictive neutrino spectrum in minimal SO(10) grand unification, [Phys. Rev. Lett. **70** \(1993\) 2845 \[hep-ph/9209215\]](#).
- [26] R.N. Mohapatra and G. Senjanovic, Neutrino Mass and Spontaneous Parity Nonconservation, [Phys. Rev. Lett. **44** \(1980\) 912](#).
- [27] M. Gell-Mann, P. Ramond and R. Slansky, Complex Spinors and Unified Theories, [Conf. Proc. C **790927** \(1979\) 315 \[1306.4669\]](#).
- [28] T. Yanagida, Horizontal gauge symmetry and masses of neutrinos, [Conf. Proc. C **7902131** \(1979\) 95](#).
- [29] P. Minkowski, $\mu \rightarrow e\gamma$ at a Rate of One Out of 10^9 Muon Decays?, [Phys. Lett. B **67** \(1977\) 421](#).
- [30] S. Bertolini, L. Di Luzio and M. Malinsky, Intermediate mass scales in the non-supersymmetric SO(10) grand unification: A Reappraisal, [Phys. Rev. D **80** \(2009\) 015013 \[0903.4049\]](#).
- [31] B. Dutta, Y. Mimura and R.N. Mohapatra, Neutrino masses and mixings in a predictive SO(10) model with CKM CP violation, [Phys. Lett. B **603** \(2004\) 35 \[hep-ph/0406262\]](#).

- [32] J. Chakraborty, R. Maji, S.K. Patra, T. Srivastava and S. Mohanty, Roadmap of left-right models based on GUTs, *Phys. Rev. D* **97** (2018) 095010 [[1711.11391](#)].
- [33] J. Chakraborty, R. Maji and S.F. King, Unification, Proton Decay and Topological Defects in non-SUSY GUTs with Thresholds, *Phys. Rev. D* **99** (2019) 095008 [[1901.05867](#)].
- [34] Z.-z. Xing, H. Zhang and S. Zhou, Impacts of the Higgs mass on vacuum stability, running fermion masses and two-body Higgs decays, *Phys. Rev. D* **86** (2012) 013013 [[1112.3112](#)].
- [35] G. Altarelli and G. Blankenburg, Different $SO(10)$ Paths to Fermion Masses and Mixings, *JHEP* **03** (2011) 133 [[1012.2697](#)].
- [36] W. Grimus and H. Kuhbock, Fermion masses and mixings in a renormalizable $SO(10) \times Z(2)$ GUT, *Phys. Lett. B* **643** (2006) 182 [[hep-ph/0607197](#)].
- [37] W. Grimus and H. Kuhbock, A renormalizable $SO(10)$ GUT scenario with spontaneous CP violation, *Eur. Phys. J. C* **51** (2007) 721 [[hep-ph/0612132](#)].
- [38] B. Dutta, Y. Mimura and R.N. Mohapatra, Suppressing proton decay in the minimal $SO(10)$ model, *Phys. Rev. Lett.* **94** (2005) 091804 [[hep-ph/0412105](#)].
- [39] Z.-z. Xing, H. Zhang and S. Zhou, Updated Values of Running Quark and Lepton Masses, *Phys. Rev. D* **77** (2008) 113016 [[0712.1419](#)].
- [40] K.S. Babu, B. Bajc and S. Saad, Yukawa Sector of Minimal $SO(10)$ Unification, *JHEP* **02** (2017) 136 [[1612.04329](#)].
- [41] I. Esteban, M.C. Gonzalez-Garcia, M. Maltoni, T. Schwetz and A. Zhou, The fate of hints: updated global analysis of three-flavor neutrino oscillations, *JHEP* **09** (2020) 178 [[2007.14792](#)].
- [42] G.C. Branco, R. Gonzalez Felipe, F.R. Joaquim and M.N. Rebelo, Leptogenesis, CP violation and neutrino data: What can we learn?, *Nucl. Phys. B* **640** (2002) 202 [[hep-ph/0202030](#)].
- [43] E. Nezri and J. Orloff, Neutrino oscillations versus leptogenesis in $SO(10)$ models, *JHEP* **04** (2003) 020 [[hep-ph/0004227](#)].
- [44] P. Di Bari and A. Riotto, Successful type I Leptogenesis with $SO(10)$ -inspired mass relations, *Phys. Lett. B* **671** (2009) 462 [[0809.2285](#)].
- [45] P. Di Bari and A. Riotto, Testing $SO(10)$ -inspired leptogenesis with low energy neutrino experiments, *JCAP* **04** (2011) 037 [[1012.2343](#)].
- [46] A. Dueck and W. Rodejohann, Fits to $SO(10)$ Grand Unified Models, *JHEP* **09** (2013) 024 [[1306.4468](#)].
- [47] C.S. Fong, D. Meloni, A. Meroni and E. Nardi, Leptogenesis in $SO(10)$, *JHEP* **01** (2015) 111 [[1412.4776](#)].
- [48] V.S. Mummidi and K.M. Patel, Leptogenesis and fermion mass fit in a renormalizable $SO(10)$ model, *JHEP* **12** (2021) 042 [[2109.04050](#)].
- [49] R. Barbieri, P. Creminelli, A. Strumia and N. Tetradis, Baryogenesis through leptogenesis, *Nucl. Phys.* **B575** (2000) 61 [[hep-ph/9911315](#)].
- [50] A. Abada, S. Davidson, F.-X. Josse-Michaux, M. Losada and A. Riotto, Flavor issues in leptogenesis, *JCAP* **04** (2006) 004 [[hep-ph/0601083](#)].

- [51] A. De Simone and A. Riotto, On the impact of flavour oscillations in leptogenesis, *JCAP* **0702** (2007) 005 [[hep-ph/0611357](#)].
- [52] S. Blanchet, P. Di Bari and G.G. Raffelt, Quantum Zeno effect and the impact of flavor in leptogenesis, *JCAP* **0703** (2007) 012 [[hep-ph/0611337](#)].
- [53] S. Blanchet, P. Di Bari, D.A. Jones and L. Marzola, Leptogenesis with heavy neutrino flavours: from density matrix to Boltzmann equations, *JCAP* **1301** (2013) 041 [[1112.4528](#)].
- [54] L. Covi, E. Roulet and F. Vissani, CP violating decays in leptogenesis scenarios, *Phys. Lett. B* **384** (1996) 169 [[hep-ph/9605319](#)].
- [55] PLANCK collaboration, Planck 2015 results. XIII. Cosmological parameters, *Astron. Astrophys.* **594** (2016) A13 [[1502.01589](#)].
- [56] K. Moffat, S. Pascoli, S.T. Petcov, H. Schulz and J. Turner, Three-flavored nonresonant leptogenesis at intermediate scales, *Phys. Rev. D* **98** (2018) 015036 [[1804.05066](#)].
- [57] A. Granelli, K. Moffat, Y.F. Perez-Gonzalez, H. Schulz and J. Turner, ULYSSES: Universal LeptogeneSiS Equation Solver, *Comput. Phys. Commun.* **262** (2021) 107813 [[2007.09150](#)].
- [58] M. Beneke, B. Garbrecht, M. Herranen and P. Schwaller, Finite Number Density Corrections to Leptogenesis, *Nucl. Phys. B* **838** (2010) 1 [[1002.1326](#)].
- [59] LEGEND Collaboration, N. Abgrall, I. Abt, M. Agostini, A. Alexander, C. Andreoiu et al., Legend-1000 preconceptual design report, 2021. [10.48550/ARXIV.2107.11462](#).
- [60] G. Adhikari, S.A. Kharusi, E. Angelico, G. Anton, I.J. Arnquist, I. Badhrees et al., nexo: neutrinoless double beta decay search beyond 10^{28} year half-life sensitivity, *Journal of Physics G: Nuclear and Particle Physics* **49** (2021) 015104.
- [61] J.J. Gomez-Cadenas, Status and prospects of the next experiment for neutrinoless double beta decay searches, 2019. [10.48550/ARXIV.1906.01743](#).
- [62] F. Agostini, S.E.M.A. Maouloud, L. Althueser, F. Amaro, B. Antunovic, E. Aprile et al., Sensitivity of the darwin observatory to the neutrinoless double beta decay of ^{136}Xe , .
- [63] S. Andringa, E. Arushanova, S. Asahi, M. Askins, D.J. Auty, A.R. Back et al., Current status and future prospects of the SNO+ experiment, *Advances in High Energy Physics* **2016** (2016) 1.
- [64] E. Armengaud, C. Augier, A.S. Barabash, F. Bellini, G. Benato, A. Benoît et al., The CUPID-mo experiment for neutrinoless double-beta decay: performance and prospects, *The European Physical Journal C* **80** (2020) .
- [65] G. Lazarides, R. Maji and Q. Shafi, Cosmic strings, inflation, and gravity waves, *Phys. Rev. D* **104** (2021) 095004 [[2104.02016](#)].
- [66] G. Lazarides, R. Maji and Q. Shafi, Gravitational waves from quasi-stable strings, *JCAP* **08** (2022) 042 [[2203.11204](#)].
- [67] R. Maji and Q. Shafi, Monopoles, Strings and Gravitational Waves in Non-minimal Inflation, [2208.08137](#).
- [68] T. Vachaspati and A. Vilenkin, Gravitational Radiation from Cosmic Strings, *Phys. Rev. D* **31** (1985) 3052.
- [69] A. Vilenkin, Cosmic Strings and Domain Walls, *Phys. Rept.* **121** (1985) 263.

- [70] Y. Cui, M. Lewicki, D.E. Morrissey and J.D. Wells, Probing the pre-BBN universe with gravitational waves from cosmic strings, *JHEP* **01** (2019) 081 [[1808.08968](#)].
- [71] J.J. Blanco-Pillado and K.D. Olum, Stochastic gravitational wave background from smoothed cosmic string loops, *Phys. Rev. D* **96** (2017) 104046 [[1709.02693](#)].
- [72] J.J. Blanco-Pillado, K.D. Olum and B. Shlaer, The number of cosmic string loops, *Phys. Rev. D* **89** (2014) 023512 [[1309.6637](#)].
- [73] LISA collaboration, Laser Interferometer Space Antenna, [1702.00786](#).
- [74] W.-H. Ruan, Z.-K. Guo, R.-G. Cai and Y.-Z. Zhang, Taiji Program: Gravitational-Wave Sources, [1807.09495](#).
- [75] TIANQIN collaboration, TianQin: a space-borne gravitational wave detector, *Class. Quant. Grav.* **33** (2016) 035010 [[1512.02076](#)].
- [76] V. Corbin and N.J. Cornish, Detecting the cosmic gravitational wave background with the big bang observer, *Class. Quant. Grav.* **23** (2006) 2435 [[gr-qc/0512039](#)].
- [77] N. Seto, S. Kawamura and T. Nakamura, Possibility of direct measurement of the acceleration of the universe using 0.1-Hz band laser interferometer gravitational wave antenna in space, *Phys. Rev. Lett.* **87** (2001) 221103 [[astro-ph/0108011](#)].
- [78] MAGIS collaboration, Mid-band gravitational wave detection with precision atomic sensors, [1711.02225](#).
- [79] AEDGE collaboration, AEDGE: Atomic Experiment for Dark Matter and Gravity Exploration in Space, *EPJ Quant. Technol.* **7** (2020) 6 [[1908.00802](#)].
- [80] L. Badurina et al., AION: An Atom Interferometer Observatory and Network, *JCAP* **05** (2020) 011 [[1911.11755](#)].
- [81] B. Sathyaprakash et al., Scientific Objectives of Einstein Telescope, *Class. Quant. Grav.* **29** (2012) 124013 [[1206.0331](#)].
- [82] LIGO SCIENTIFIC collaboration, Exploring the Sensitivity of Next Generation Gravitational Wave Detectors, *Class. Quant. Grav.* **34** (2017) 044001 [[1607.08697](#)].
- [83] L. Lentati et al., European Pulsar Timing Array Limits On An Isotropic Stochastic Gravitational-Wave Background, *Mon. Not. Roy. Astron. Soc.* **453** (2015) 2576 [[1504.03692](#)].
- [84] G. Janssen et al., Gravitational wave astronomy with the SKA, *PoS AASKA14* (2015) 037 [[1501.00127](#)].
- [85] GAIA collaboration, Gaia Data Release 2, *Astron. Astrophys.* **616** (2018) A1 [[1804.09365](#)].
- [86] THEIA collaboration, Theia: Faint objects in motion or the new astrometry frontier, [1707.01348](#).
- [87] Z.-C. Chen, Y.-M. Wu and Q.-G. Huang, Search for the Gravitational-wave Background from Cosmic Strings with the Parkes Pulsar Timing Array Second Data Release, [2205.07194](#).
- [88] J. Ellis and M. Lewicki, Cosmic String Interpretation of NANOGrav Pulsar Timing Data, *Phys. Rev. Lett.* **126** (2021) 041304 [[2009.06555](#)].